

The Chance of Freezing – ~~Parameterizing temperature-dependent~~ A conceptual study to parameterize temperature-dependent freezing by including randomness of INP concentrations

Hannah C. Frostenberg¹, André Welti², Mikael Luhr³, Julien Savre⁴, Erik S. Thomson⁵, and Luisa Ickes¹

¹Department of Space, Earth and Environment, Chalmers University, Gothenburg 41296, Sweden

²Finnish Meteorological Institute, Helsinki 00101, Finland

³former Department of Meteorology, Stockholm University, Stockholm 10691, Sweden

⁴Meteorological Institute, Faculty of Physics, Ludwig-Maximilians-Universität, Munich 80333, Germany

⁵Department of Chemistry and Molecular Biology, University of Gothenburg, Gothenburg 41296, Sweden

Correspondence: Hannah Frostenberg (hannah.frostenberg@chalmers.se), Luisa Ickes (luisa.ickes@chalmers.se)

Abstract. Ice nucleating particle (~~INP~~-~~concentrations~~-concentrations (INPCs) can spread over several orders of magnitude at any given temperature. However, this variability is rarely accounted for in heterogeneous ice nucleation parameterizations. We developed a scheme for immersion freezing where the ~~INP-concentration~~-INPC is drawn from a relative frequency distribution of cumulative ~~INP-concentrations~~INPCs. At each temperature, this distribution describing the ~~INP-concentrations~~-INPCs is expressed as a log-normal frequency distribution. The new parameterization scheme does not require aerosol information from the driving model to represent the heterogeneity of ~~INP-concentrations~~INPCs. The scheme's performance is tested in a large-eddy simulation of ~~an Arctic~~-a relatively warm Arctic mixed-phase stratocumulus. We find that it leads to reasonable ice masses in the cloud, especially compared to immersion freezing schemes that yield one fixed INPC per temperature and lead to almost no ice production in the simulated cloud. The scheme is sensitive to the median of the frequency distribution and highly sensitive to the standard deviation of the distribution, as well as to the frequency of drawing a new INPC and the resolution of the model. Generally, ~~larger~~-higher probability to draw ~~high-INP-concentrations~~-large INPCs leads to substantially more ice in the simulated cloud. We expose inherent challenges to introducing such a parameterization and explore possible solutions and potential developments.

1 Introduction

Clouds play an important role in Earth's energy balance by reflecting incoming sunlight and interacting with infrared radiation. The cloud phase influences the amount of a cloud's radiative effect, but more importantly, it determines whether the cloud has a warming or cooling effect. According to Matus and L'Ecuyer (2017), liquid clouds have a global net radiative effect at the top-of-atmosphere (TOA) of -11.8 W m^{-2} , whereas ice clouds exert a warming of 3.5 W m^{-2} and mixed-phase clouds cause a net cooling effect of -3.4 W m^{-2} .

The ice crystals in mixed-phase clouds usually originate from heterogeneous ice nucleation where ice nucleating particles (INPs) are necessary to trigger the phase transition. Ice nucleates heterogeneously in the atmosphere ~~for~~-at temperatures be-

tween 0 and approximately -38°C . At temperatures below -38°C , homogeneous ice nucleation occurs spontaneously and freezing can happen without INPs. Heterogeneous ice nucleation can occur in different so-called modes: immersion freezing, contact freezing, deposition nucleation, and condensation freezing (see Vali et al., 2015, for definitions). We focus on immersion freezing where an INP is immersed in a supercooled cloud droplet and initiates freezing at a specific temperature. ~~Contact freezing, deposition nucleation and condensation freezing are further heterogeneous nucleation modes (see Vali et al., 2015, for definitions)~~ Different aerosol types can act as INPs: mineral dusts, biological and combustion particles, etc. The probability that an aerosol initiates ice nucleation increases with decreasing temperature. Measurements of ambient INP concentrations (INPC [m^{-3}]) show that at a given temperature, INPC can vary by several orders of magnitude, over time and space. ~~An example for~~ Examples of spatial INPC variability in different marine locations, from approximately 10^{-1} to 10^3 m^{-3} at -15°C can be found in Welti et al. (2020). Temporal variability, for example, the annual cycle of INPC in the Arctic, was reported to be up to three orders of magnitude (Wex et al., 2019). But also within smaller time periods down to single days, the INPC can fluctuate by up to three orders of magnitude (Bigg, 1961). It has been found that the INPC at a specific temperature is log-normally distributed. Log-normal frequency distributions of INPC occurrence have been measured at several locations within different environments (e.g., Isaac and Douglas, 1971; Bertrand et al., 1973; Radke et al., 1976; Flyger and Heidam, 1978; Conen et al., 2017; Welti et al., 2018; Hartmann et al., 2019; Schrod et al., 2020; Li et al., 2022). Ott (1990) showed that when an aerosol concentration is observed to have a log-normally distributed occurrence this likely results because the aerosol was subject to a series of random dilutions subsequent to emission.

Several parameterizations that simulate cloud droplet freezing exist and they are based on different physical variables. Burrows et al. (2022) distinguish between aerosol-aware and -unaware parameterizations. One example of the latter is the formulation by Fletcher (1962) (F62); a scheme that ~~only requires temperature information to calculate INPC. F62~~ is based on the observation that ~~while the INPC varies from day to day and place to place, the average~~ the average INP concentration increases exponentially with decreasing temperature for $-10 > T > -30^{\circ}\text{C}$. F62 only requires temperature information to calculate INPC. The scheme by Niemand et al. (2012) (N12) is an example of an aerosol-aware parameterization, ~~since~~; it describes immersion freezing based on the active site density of desert dust aerosols observed in laboratory measurements. N12 is valid ~~from~~ for -12 ~~to~~ $T > -36^{\circ}\text{C}$ and requires temperature, the number of dust aerosols, and the average INP surface ~~and temperature~~ as input to determine INPC. Another example of an aerosol-aware scheme is the parameterization by Phillips et al. (2008) (P08) which represents immersion, contact, and deposition freezing on dust/metal aerosol, organic carbon, and biological INPs. P08 uses temperature, water ~~vapour~~ vapor saturation with respect to ice, and aerosol concentrations of the four aerosol species to predict INPC. P08 is valid for ~~temperatures between 0 and~~ $T > -70^{\circ}\text{C}$ (or lower). The parameterization of Khvorostyanov and Curry (2000) (K00) is based on classical nucleation theory (CNT), where each substance is assigned a characteristic contact angle between a nucleating ice cluster and the particle surface. The smaller the contact angle, the more ~~ice active~~ ice-active a substance. K00 utilizes temperature, water ~~vapour~~ vapor saturation with respect to ice, particle radius, and one contact angle per substance to calculate ice nucleation rates. One method of including ~~particle to particle~~ particle-to-particle heterogeneity of INPs in parameterizations is to apply a distribution on the contact angle parameter in CNT to calculate the ice-activity of the INPs (e.g., Marcolli et al., 2007 or Wang et al., 2014). These schemes ~~use~~ require temperature and aerosol ~~size distributions as~~

~~input from the atmospheric model~~ radius as input to the parameterization and use different values for the mean and standard deviation of the contact angle distribution for different aerosol species.

There are three drawbacks that ice nucleation parameterizations can have: i. They can be computationally complex, i.e., require
60 detailed input from ~~the model regarding models regarding the~~ aerosol type, size, and/or number concentration. ii. They ~~often are valid only for a limited~~ can be limited to a specific temperature range. iii. ~~They~~ Most of them fail to reproduce INPC variability, i.e., for one set of environmental conditions (temperature, humidity, aerosol type, and concentration) they yield ~~one~~ a single fixed INPC value.

The lack of INPC variability in simulations compared to atmospheric observations ~~comes from~~ emerges from non-represented
65 INP types and sources, the large size of model grid boxes, and the use of bulk aerosol concentrations (e.g., dust, soot, biological) as input variables in parameterizations. Even if a model ~~had~~ includes information on, e.g., the detailed size distribution of dust aerosol, it will not represent all the ~~different~~ dust INP types (different minerals) and their variability ~~that are present~~ in the atmosphere. To circumvent these drawbacks we developed a parameterization of immersion freezing (~~F22~~F23) that simulates observed INPC and their variability while only using temperature as input variable. ~~F22~~F23 is valid for the entire temperature
70 range of immersion freezing (~~from 0 to~~ $T > -38^{\circ}\text{C}$). The INPCs returned by ~~F22~~F23 are drawn randomly from a log-normal distribution of INPCs for each temperature, thereby capturing the natural INP variability, without requiring information about the present ~~bulk aerosol. Log-normal distributions of INPCs have been observed at several locations with different environments~~ (ice-active aerosol. The random drawing allows to represent the INP population by a distribution of INPCs, instead of, e.g.,
75 ~~Isaac and Douglas, 1971; Bertrand et al., 1973; Radke et al., 1976; Flyger and Heidam, 1978; Conen et al., 2017; Welts et al., 2018~~ ; Hartmann et al., 2019; Schrod et al., 2020; Li et al., 2022). The ~~similarity to a log-normal distribution indicates that the measured INPCs were subject to random dilutions since their emission into the atmosphere (Ott, 1990)~~ one single value as in F62. The log-normal ~~distribution F22 is based upon has been found in observations~~ INPC distributions F23 is loosely based upon have been observed in the maritime boundary layer (see ~~See~~ 2Sect. 2).

We ~~tested the performance of the new F22~~ test the new F23 parameterization in the large-eddy simulation (LES) model MI-
80 MICA (MISU/MIT Cloud-Aerosol model, Savre et al., 2014) to ~~confirm that it produces a reasonable amount of~~ investigate how it performs at producing ice in a simulated cloud ~~and analyzed in comparison to conventional parameterizations (diagnostic ice crystal number concentration, and F62)~~. We analyze the sensitivity of the scheme on its characteristics and implementation details. The simulations are initialized based on in-situ observations during the ASCOS (Arctic Summer Cloud Ocean Study) Arctic campaign and represent a mixed-phase stratocumulus cloud with in-cloud temperatures between approximately -7 and
85 -10°C (see ~~See~~ 2Sect. 2.2).

2 Method

2.1 Formulation of the ~~F22~~F23 parameterization

The ~~F22 parameterization for immersion freezing is based on i.~~ basic idea for the new F23 parameterization is that INPCs have large variability, even on short time scales (Bigg, 1961), which we represent by drawing a new INPC from the given

90 distribution at a certain frequency if immersion freezing occurs (i.e., $T < 0^\circ\text{C}$ and cloud droplets are present). Drawing a new INPC mimics the evolution of the ice-active aerosol population, for example by replenishment or time-dependent freezing at each grid point. The latter means that drawing at each time step does not necessarily reflect a change in aerosol population from one time step to another, but a change in the present INP population due to the activation of more INPs with time. The main goal of this study is to test the concept of randomly drawing from a distribution of INPCs instead of applying a deterministic value (e.g., the median of observed INPCs) as is done in other freezing parameterization schemes.

95 We use the conceptual distribution of INPCs shown in Fig. 1, derived from the extensive data sets of a long-term time series of INPC temperature spectra measured in the maritime boundary layer at Cabo Verde (Welti et al., 2018) and ii. wide-area widely dispersed ship-based observations (Welti et al., 2020). The observations were made by collecting INPs on filters and subsequent drop-freezing experiments at temperatures from 0 to -26°C , and using a continuous flow diffusion chamber for low-temperature observations (-24 to -38°C). On average there is

100 On average, the INPC field observations show a striking consistency of the temperature spectra's shape and variability over time and location. The same consistencies exist in-comparison when compared with other long-term (e.g. Schrod et al., 2020) or composite INPC data sets (e.g. Petters and Wright, 2015).

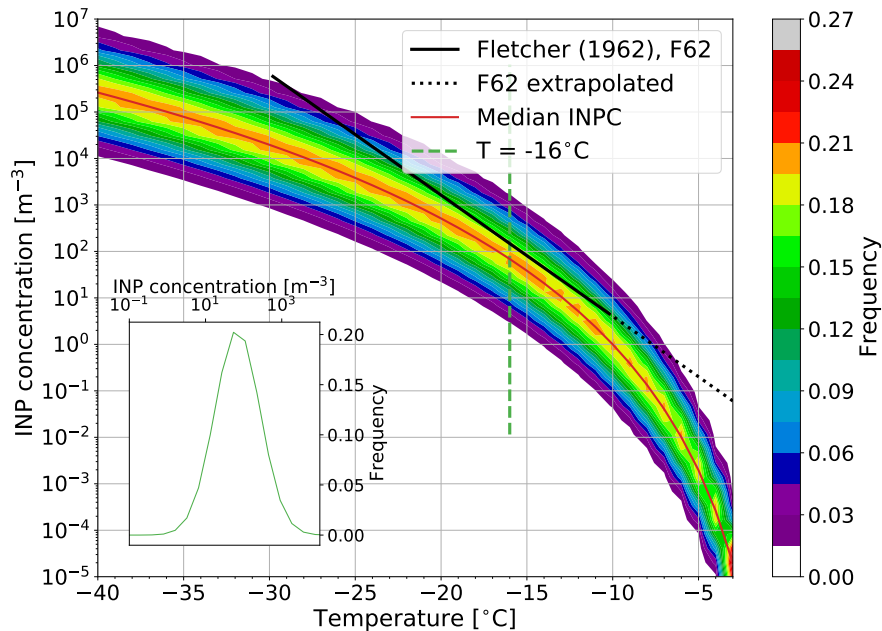


Figure 1. Relative frequency distribution (RFD) spectra for INPC as a function of temperature. Median INPCs are marked by the red line. The log-linear parameterization by Fletcher (1962) (F62) is shown within its validity range (black solid) and extrapolated to higher temperatures (black dotted) for comparison. The inset in the lower left corner shows the RFD at $T = -16^\circ\text{C}$ (green dashed line).

Based on the aforementioned data sets, we derived Relative frequency distribution spectra for INPC as a function of temperature. The log-linear parameterization by Fletcher (1962) within its validity range is shown for comparison. The inset in the lower

105 ~~left corner shows the RFD at $T = -16^\circ\text{C}$ (dashed line):~~ a function for temperature-dependent, log-normally distributed INPC frequency:

$$D(\mu, \sigma^2) = \frac{1}{\sqrt{2\pi} \cdot \sigma} \exp \left(- \frac{[\ln(\text{INPC}) - \mu]^2}{2\sigma^2} - \frac{[\ln(a \cdot \text{INPC}) - \mu(T)]^2}{2\sigma^2} \right), \quad (1)$$

with $a = 1 \text{ m}^3 \text{ INPC in m}^{-3}$, $\mu(T)$ the ~~temperature-dependent mean~~ temperature-dependent mean, and σ^2 the variance of the log-normal distribution (not the INPC itself). For the marine data sets we find $\sigma = 1.37$ and $\mu(T) = \ln(-T^9 \cdot 10^{-9})$ with $\mu(T) = \ln(-(b \cdot T)^9 \cdot 10^{-9})$ with $b = 1/(1^\circ\text{C})$ and T given in $^\circ\text{C}$. By normalizing the distribution, a relative frequency distribution (RFD) as a function of temperature is obtained (Fig. 1). Whenever ~~a~~ an immersion freezing event occurs in the model (i.e., $T \leq 0^\circ\text{C}$ and ~~saturation with respect to ice, $s_i \geq 1$~~ cloud droplets are present), an INPC value is drawn randomly from the RFD. That is, for two grid points with freezing events at the same temperature, the drawn INPC can differ by several orders of magnitude. For a large number of grid points, the relative frequency of the drawn INPC will follow a log-normal function with the median INPC (~~orange region~~ red line in Fig. 1) having the highest probability. For example, if all grid points ~~had the temperature were at a temperature of~~ -16 $^\circ\text{C}$, the frequency of the ~~picked drawn~~ INPC would follow the ~~green curve shown~~ distribution shown as a green curve in the lower left Fig. 1 inset.

~~F22-F23~~ assumes that all INPs are immersed in cloud droplets. To take into account the dynamic evolution of ice formation, the ice crystal number concentration (N_i) at the a grid point is subtracted from the drawn INPC. This returns the number of newly frozen cloud droplets in the a time step, i.e., hydrometeors moving from class *cloud droplet* to class *ice crystal*. Subtracting N_i is one approach to solve the need for time discretization when implementing a deterministic time-independent scheme. Note that if other frozen hydrometeor species (snow, graupel) are represented in the model (not implemented in our setup), the sum of their number concentrations should be subtracted from the drawn INPC. No negative tendencies ($\text{INPC} - N_i < 0$) are allowed in the scheme, since already frozen cloud droplets will not melt due to a decrease in ~~INPs~~ the INPC. The change in the respective mixing ratios is calculated by multiplying the change in the number of frozen droplets by the average cloud droplet mass:

$$\Delta N_i = -\Delta N_c = \max([\text{INPC} - N_i], 0), \quad (2a)$$

$$\Delta Q_i = -\Delta Q_c = \Delta N_i \frac{\overline{Q_c}}{\overline{N_c}}. \quad (2b)$$

Here, N_i and N_c are the ice crystal and cloud droplet number concentrations, ~~respectively in m^{-3}~~ , Q_i and Q_c are the ice crystal and cloud droplet mixing ratios in kg m^{-3} , respectively, ~~and with~~ the mean cloud droplet mixing ratio and number concentration ~~are~~ denoted by the bar. The calculations are repeated at each time step, which means that INPs are only partially depleted through the subtraction of N_i . We ~~see~~ interpret this as a way to imitate ~~time-dependent~~ time-dependent freezing and INP ~~eyelining~~ recycling, which has been shown to be crucial for realistic cloud development in LES for Arctic mixed-phase clouds (e.g., Solomon et al., 2015).

135 The implemented INPC RFD-field is discretized into bins of INPC and temperature. The INPCs differ approximately by a factor of 2 (or $\Delta \log_{10}(\text{INPC}) \approx \log_{10}(2)$), while the temperature bins have a size of 1°C . ~~This is why $^\circ\text{C}$. For this reason,~~ we

define temperature to the nearest degree when drawing from the INPC RFD if not stated otherwise. Using the F23 immersion freezing scheme in MIMICA has approximately the same computational expense for the total simulation time as any other interactive ice nucleation parameterization, for example, F62.

140 2.1.1 Example of parameterized INP concentrations

To illustrate the INPC distribution from the ~~F22~~ F23 parameterization, let us assume that we have a uniform -16°C cloud ~~horizontally spreading~~ spreading horizontally over the entire model domain consisting of 1000 grid points. ~~In this case, the~~ The INPC RFD at all cloud grid points is represented by a log-normal distribution curve (inset in Fig. 1). ~~That means that This~~ results in an INPC of ~~approximately~~ 68.7 m^{-3} ~~will be being~~ drawn with the highest probability, since this is the median INPC: ~~Med[INPC($T = -16^{\circ}\text{C}$)] = $\exp(\mu) = -T^9 \cdot 10^{-9} \approx 68.7$ at -16°C : Med[INPC($T = -16^{\circ}\text{C}$)] = $\exp(\mu)\text{ m}^{-3} = -T^9 \cdot 10^{-9}\text{ m}^{-3} \approx 68.7\text{ m}^{-3}$~~ Med[INPC($T = -16^{\circ}\text{C}$)] = $\exp(\mu) = -T^9 \cdot 10^{-9} \approx 68.7$ at -16°C : Med[INPC($T = -16^{\circ}\text{C}$)] = $\exp(\mu)\text{ m}^{-3} = -T^9 \cdot 10^{-9}\text{ m}^{-3} \approx 68.7\text{ m}^{-3}$ ~~In the model,~~ In the model, 20.2% of the grid points will draw the median INPC, ~~so that is~~ so that is 202 of the 1000 cloud grid points ~~are expected to~~ will get the median INPC of 54.3 m^{-3} (differing from the theoretical value of 68.7 m^{-3} because of discrete INPC ~~bins~~ binning). The range of INPC bins with a relative frequency $> 0.1\%$ covers INPCs of $0.8 - 7543.1\text{ m}^{-3}$, which means that ~~neither rarely~~ neither rarely INPCs ≤ 0.8 ~~nor or~~ nor or $\geq 7543.1\text{ m}^{-3}$ will be drawn ~~in for~~ in for the example cloud. If no ice was present previously, the ~~INPC equals~~ INPC equals ~~the~~ the number of cloud droplets frozen at this time step equals the INPC (Eq. 2a), limited by the total number of cloud droplets present.

2.1.2 Representing the RFD

Since the parameterization draws values from a distribution, it needs to be ensured that there are enough random draws ~~at~~ at ~~each time step~~ each time step in order to represent the distribution well: INPCs in the model should vary according to the distribution, but ~~different model runs should also be reproducible.~~ different model runs should also be reproducible. To investigate how many draws are necessary ~~for a “good” representation~~ for a “good” representation ~~of the INPC distribution to represent the INPC distribution,~~ of the INPC distribution to represent the INPC distribution, we conducted several drawing tests (drawing, e.g., 50 times from the distribution vs. drawing 100 times) at -16°C and compared the relative frequencies of the drawn values to the theoretical ~~ones values~~ ones values by calculating the root mean square error (RMSE) between the drawn and theoretical distributions. Comparing the results of the different drawing tests suggests that 300 random draws lead to a reproducible prediction of the RFD (see ~~Table 1 and Fig. 2);~~ Table 1 and Fig. 2); the RMSE converges for ≥ 300 with a constant first derivative (linear slope) of the connecting lines, and the standard deviation decreases only slightly for > 300 draws.

The domain used in the simulations has 96×96 grid points in the horizontal, leading to 9216 grid points in each layer. The simulated cloud is stratocumulus (see ~~Sec. 2.2~~ Sect. 2.2), where the temperature field is ~~very uniform in the horizontal~~ horizontally uniform. Assuming that at least one layer of grid points in the model has the same temperature due to the uniform structure of the stratus cloud, this translates into a minimum of 9216 grid points with the same temperature. This implies a minimum of 9216 draws from the RFD at one temperature, which is substantially more than the minimum number of draws determined to well-represent the distribution (300). Hence, we confirm that a representative INPC distribution is being drawn from the RFD. This has also been verified in MIMICA simulations (not shown).

Table 1. Average and standard deviation of RMSE for different draw amounts from the INPC RFD at -16°C compared to theoretical RFD values. Each drawing test was performed 100 times and the table contains the average and standard deviation of the RMSE over these 100 times.

Number of draws	Mean RMSE [m^{-3}]	Standard deviation RMSE [m^{-3}]
50	$17.8 \cdot 10^{-3}$	$5.47 \cdot 10^{-3}$
100	$12.4 \cdot 10^{-3}$	$3.51 \cdot 10^{-3}$
200	$8.65 \cdot 10^{-3}$	$2.58 \cdot 10^{-3}$
300	$7.28 \cdot 10^{-3}$	$2.03 \cdot 10^{-3}$
400	$6.26 \cdot 10^{-3}$	$1.59 \cdot 10^{-3}$
500	$5.67 \cdot 10^{-3}$	$1.40 \cdot 10^{-3}$
600	$5.27 \cdot 10^{-3}$	$1.49 \cdot 10^{-3}$
700	$4.77 \cdot 10^{-3}$	$1.39 \cdot 10^{-3}$
800	$4.45 \cdot 10^{-3}$	$1.19 \cdot 10^{-3}$
900	$4.18 \cdot 10^{-3}$	$1.08 \cdot 10^{-3}$
1000	$3.73 \cdot 10^{-3}$	$1.11 \cdot 10^{-3}$

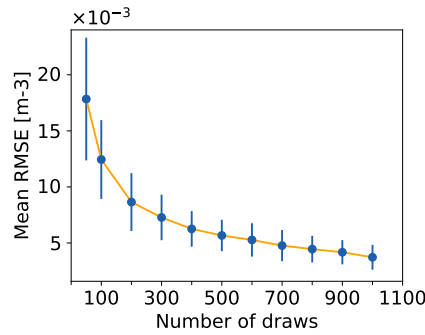


Figure 2. Average and standard deviation of RMSE for the drawing tests in Table 1 are decreasing for increasing number of draws at -16°C .

2.1.3 Performance of the parameterization scheme in MIMICA

170 Using the F22 immersion freezing scheme approximately doubles the computational expense compared to the standard MIMICA setup where ice nucleation is not represented explicitly, i.e., runs without an explicit freezing parameterization (instead the ice crystal number concentration (N_i) is kept constant). The computational expense of applying F22 is similar to using other freezing parameterizations like N12 (Niemand et al., 2012).

2.2 Simulation setup

175 We use the well-established large-eddy simulation (LES) model MIMICA (MISU/MIT Cloud-Aerosol model, Savre et al., 2014). For more information on the model, see additionally Appendix A or, e.g., Savre and Ekman (2015a), Savre and Ekman (2015b), or Sotiropoulou et al. (2020). The simulated case is based on a mixed-phase Arctic stratocumulus. The case-study

stratocumulus cloud was observed between 30 August and 31 August 2008 during the ship-based ASCOS campaign (Arctic Summer Cloud Ocean Study; Tjernström et al., 2014). At that time, the research vessel Oden was drifting with an ~~ice-floe-ice~~ floe located at approximately 87° N. The atmospheric conditions were characterized by a high-pressure system with large-scale subsidence in the free troposphere (for details see Tjernström et al., 2012). This case has been used to study other microphysical cloud properties like dissipation (Loewe et al., 2017), the influence of CCN hygroscopicity on cloud properties (Christiansen et al., 2020), secondary ice production (Sotiropoulou et al., 2021) and sustenance (Bulatovic et al., 2021) of an Arctic ~~mixed phase-mixed-phase~~ cloud, as well as in a model intercomparison study (Stevens et al., 2018). We selected this case ~~because~~ it is an established case and because there are large uncertainties about the nature and concentration of INPs in the Arctic, which poses a challenge to modeling mixed-phase clouds in this region. Using other immersion freezing parameterizations in MIMICA, for example, an active site scheme following Ickes et al. (2017), to simulate this case requires unrealistically active INPs in order to form ice. We focus on immersion freezing in this study because liquid-dependent ice nucleation is dominant in Arctic stratiform clouds (de Boer et al., 2011). Contact freezing can be neglected since very little interstitial aerosol was present in the case. Furthermore, these aerosols would need to collide with the supercooled cloud droplets in a very stable non-turbulent cloud, making contact freezing unlikely to occur. Deposition nucleation has the same limitation when it comes to interstitial aerosol and can additionally be neglected because of the temperature range which is not favorable for deposition ice nucleation. Secondary ice formation is not explicitly taken into account in this study since we focus on primary ice formation. Simulations of the case ~~without interactive ice nucleation with a diagnostic ice crystal number concentration (STD) assume a constant~~ instead of an interactive representation of ice nucleation assume a minimum ice crystal number concentration of 200 m^{-3} at grid points with a temperature below 0°C where ~~the supersaturation ratio with respect to ice is at least 0.05 and where~~ there are sufficient cloud droplets. This means that at any given time step ~~in the cloud~~ if N_i falls below 200 m^{-3} , ~~cloud droplets are converted to ice and $T < 0^\circ\text{C}$, ice crystals are produced~~ to retain $N_i = 200 \text{ m}^{-3}$, no matter the exact temperature below 0°C . This approach is unspecific to the ice formation mechanisms. It combines immersion and contact freezing (due to the requirement of cloud droplets), as well as secondary ice processes.

The MIMICA simulations are initialized with the profiles of thermodynamic variables (e.g., potential temperature and pressure) and liquid cloud water ~~that were~~ measured at approximately 06 UTC on 31 August 2008. The initial ice/liquid potential temperature profiles are randomly perturbed in order for convection to develop more quickly. Consequently, any two simulations will yield different results, even if all parameters are held constant. A cloud layer was present between ca. 550 and 900 m above ground level, capped by a temperature and humidity inversion and de-coupled from the surface (see Sotiropoulou et al., 2021 for profile details). The temperature within the cloud ranged from approximately -7 to -10°C . The simulation setup follows Sotiropoulou et al. (2021). The domain covers a $96 \times 96 \times 128$ grid with a constant horizontal spacing of $dx = dy = 62.5 \text{ m}$ ($6 \text{ km} \times 6 \text{ km}$ horizontal domain size). The vertical spacing is 7.5 m near the ground and in the cloud layer; between the surface and the cloud it changes sinusoidally and reaches a maximum dz of 25 m , with a 1.7 km total vertical domain size. The time step is dynamic in order to satisfy the ~~Courant-Friedrichs-Lewy~~ Courant-Friedrichs-Lewy (CFL) condition for the leapfrog time-integration method and ranges from $\approx 1 - 3 \text{ s}$ to prevent numerical instabilities within the model. Our simulations cover 12 hours, with the first two hours utilized as a spin-up period and subsequently omitted from the results. A large-scale steady

state is maintained throughout the model runs and the cloudy layer is present in the initial state of the simulations. However, the initial cloud is liquid and cloud ice is only formed from the first model time step.

215 We excluded the hydrometeor categories snow and graupel from ~~our simulations~~, all simulations since it is known that MIMICA produces rather large amounts of graupel for this case (Stevens et al., 2018) which dominates both ice water path (IWP) and the number concentration of frozen hydrometeors. Because we are primarily interested in ice formation in our study, ice crystals being the only frozen hydrometeors simplifies the analysis. For the same reason, snow and graupel were excluded previously from Arctic stratocumulus simulations conducted with MIMICA (Savre and Ekman, 2015b). Excluding snow and
220 graupel means that no cold collection processes are active in our simulations, however, ice crystals can still grow by deposition, be transported, and precipitate. Aerosol is not represented prognostically in the model setup.

~~For comparisons of simulations with MIMICA of the 30–31 August 2008 ASCOS case to observations, we refer to Sotiropoulou et al. (2022) and Stevens et al. (2018)~~ Observed liquid water path (LWP) and IWP were derived from measurements by a micrometer radiometer and millimeter cloud radar respectively (Tjernström et al., 2012). Uncertainties for LWP are 25 g m^{-2} while for
225 IWP they are approximately a factor of two (Shupe et al., 2013).

3 Results and discussion

We first compare the baseline version of the new ~~F22 parameterization (F22)~~ F23 parameterization (F23), all parameters are set to the values described in ~~Sect. 2.1 and Domain-averaged profiles for simulation time after 2-hour spinup-time: (a) and (e) N_i with contours of temperature, (b) and (d) ice mixing ratio (Q_i).~~ Upper row (a, b) is the STD comparison run (see dotted lines
230 in Fig. 3), lower row (c, d) is the ~~F22 comparison run (see dotted lines in Fig. 3). The dashed lines show the cloud top and bottom.~~ Sect. 2.2 Sect. 2.1) to the standard setup (STD), diagnostic ice crystal number concentration), available observations, and F62.

Domain-averaged liquid water path (LWP [g m^{-2}]), ice water path (IWP [g m^{-2}]), ice crystal number burden (ICNB [m^{-2}]) and net infrared radiation at the surface (NIRS [W m^{-2}]) for STD ~~and F22 are shown~~, F23, and F62 are shown together with
235 the median and the upper and lower quartiles of observational values for LWP and IWP in Fig. 3. The model was run ten times using STD or ~~F22 ten times~~ F23, respectively. ~~In Fig. 3, the~~ The different “ensemble members” are initialized by randomly perturbed profiles and are represented by their median, maximum, and minimum values in Fig. 3.

3.1 Comparison of F23 to STD (diagnostic ice crystal number concentration)

The F23 and STD simulations differ only in how ice crystal formation is parameterized. Other related processes like deposition and sublimation are treated in the same manner and the general setup follows Sect. 2.2. For F23, all parameters are set to the
240 values described in Sect. 2.1, while STD ensures a minimum N_i of 200 m^{-3} where the temperature is below 0°C and there are sufficient cloud droplets.

LWP is substantially larger for ~~F22~~ F23 than for STD (Fig. 3a). ~~The vertical distributions of N_c and Q_c (Fig. C1b and d) are very similar between STD and F22, which indicates that the differences in LWP are mainly caused by differences in the~~

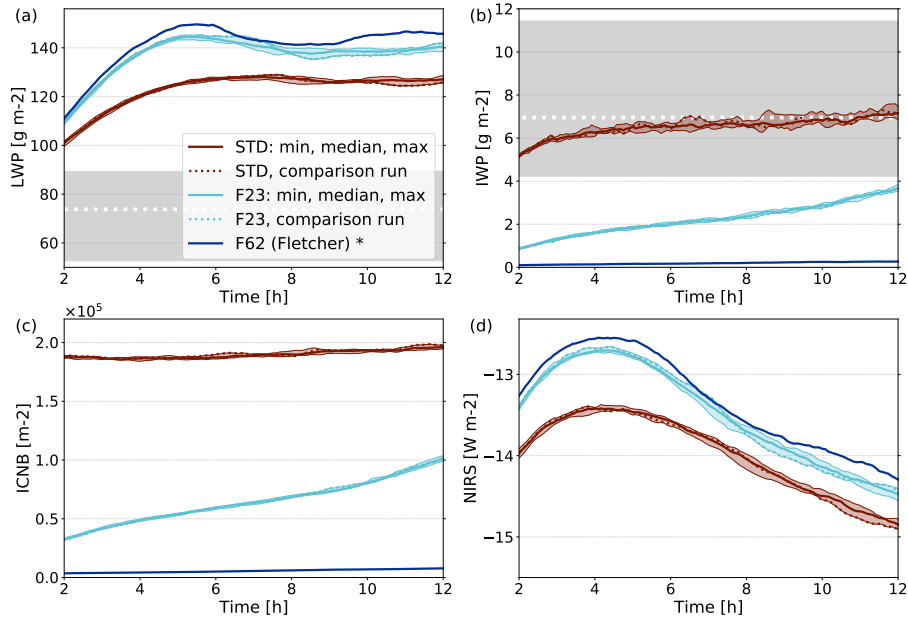


Figure 3. Domain-averaged (a) LWP, (b) IWP, (c) ice-crystal-number-burden (ICNB) and (d) net-infrared-radiation-at-surface (NIRS) for 10 simulations of STD (red; median with min/max envelope) and with the F22-F23 parameterization (cyan; median with min/max envelope). In both cases one representative simulation is plotted as a dotted line to be included in Figs. 4, D1, 6, 8, 10, 12, C1. The interquartile range of observations for LWP and IWP is indicated by the gray-shaded areas. Median observations are marked by the white dotted lines. One simulation with F62 is shown in blue. Significance was assessed with a two-sided Kolmogorov-Smirnov test at the 95% level. Significant differences in IWP of F62 to F23 are indicated with an asterisk.

245 amount-of-rain-drops. IWP is larger for STD than for F22-F23 (Fig. 3b), but does not compensate for the differences in LWP (the total mass of ice and liquid is still larger for F22-F23). The large differences in LWP between F22-F23 (INPC distribution) and STD (constant N_i) are due to enhanced freezing in STD, which leads to more latent heat release, increasing temperature and lowering supersaturation. This causes increased evaporation of liquid droplets, either with a mass flux to and deposition onto ice crystals via the Wegener-Bergeron-Findeisen process (WBF) or to the gas phase. Another cause might be a difference in turbulence with more entrainment of drier air for STD, see Fig. B1.

To analyze the ice crystal number, Fig. 3c shows the ice-crystal-number-burden (ICNB), the vertically integrated N_i (Fig. C1a). For STD, ICNB is almost constant at $1.9 \cdot 10^5$ increases slightly from $1.88 \cdot 10^5 \text{ m}^{-2}$ to $1.96 \cdot 10^5 \text{ m}^{-2}$ over 10 hours, while it increases throughout the F22 simulations from $3.5 \cdot 10^4$ dramatically throughout the F23 simulations from $3.2 \cdot 10^4 \text{ m}^{-2}$ to almost $1.0 \cdot 10^5 \text{ m}^{-2}$. ICNB has a similar slope as F22 IWP, suggesting that the average ice-crystal-mass remains constant throughout the F22 simulations. Comparing IWP and ICNB for STD, the average ice-crystal-mass increases throughout the simulation leading to different cloud situations. Several primary processes cause the increase of ice mass and number: i. The vertical extent of the liquid cloud increases throughout the simulation (see dashed lines in Fig. 4). ii. The

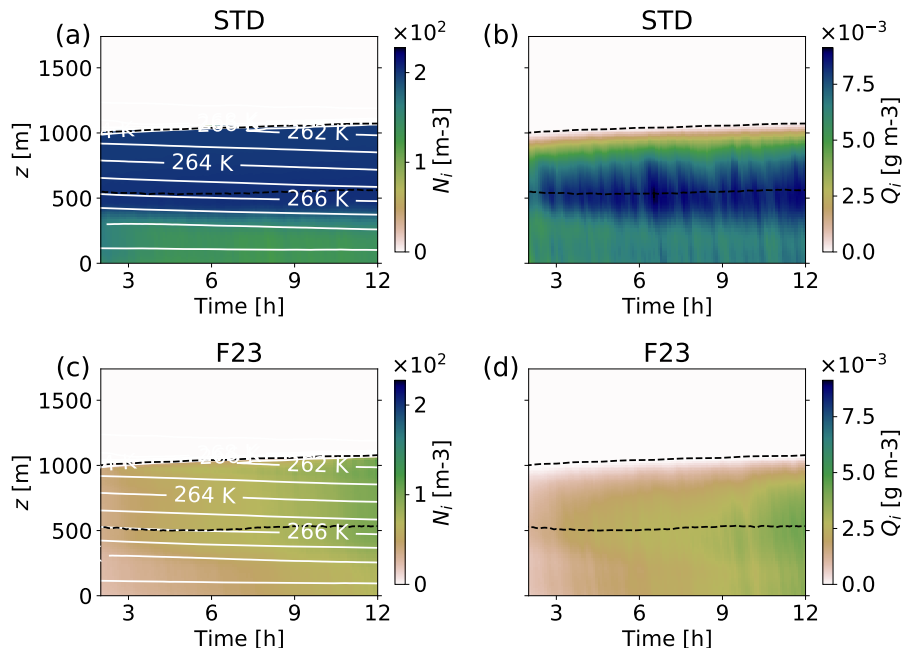


Figure 4. Domain-averaged profiles for simulation time after 2-hour spinup-time: (a) and (c) N_i with contours of temperature, (b) and (d) ice mixing ratio (Q_i). The upper row (a, b) is the STD comparison run (see red dotted lines in Fig. 3), lower row (c, d) is the F23 comparison run (see cyan dotted lines in Fig. 3). The dashed lines show the cloud's top and bottom.

temperature within the cloud decreases throughout the simulation (see white contour lines in Fig. 4a and c). iii. For F23, new ice crystals form whenever the drawn INPC is larger than the current N_i . Only process i. is relevant for STD since its requirements for ice formation are $T < 0^\circ\text{C}$ and the abundance of cloud droplets. For F23, all three processes are relevant since it requires cloud droplets (i.), the INPC RFD depends on the temperature (ii.), and iii. is an inherent characteristic.

Figure 3d shows the time series of the net infrared radiation at the surface (NIRS), i.e., incoming minus outgoing infrared radiation at the surface. NIRS is larger for F22-F23 compared to STD. This can be expected since LWP is larger for F22-F23. The evolution over time is similar in both cases, with NIRS first increasing, then decreasing from hours 4-5. This pattern emerges from the combination of first increasing, then steady LWP (for F22-F23, LWP decreases slightly between hours 5 and 8, which causes a larger decrease in NIRS), and continuously decreasing temperature (not shown) due to radiative cooling of the cloud. The variability between different realizations of either STD or F22 is shown see white lines in Fig. 3. For IWP (Fig. 3b), STD values have a larger spread than F22, while their spread is similar for the other variables. Since in STD, the ice crystal number concentration is set to a constant value where certain conditions for the temperature and supersaturation are met, fluctuations due to randomly perturbed initial conditions can have a larger effect. If several grid points are close to the supersaturation threshold, small perturbations can either cause the threshold to be exceeded and thus N_i set to 200 m^{-3} , or not to be exceeded resulting in no adaptation of N_i . This leads to a rather variable IWP for different STD runs. In contrast, for

F22 the variation between the drawn INPCs at different grid points can be large in any simulation, because a large number of freezing events happens at each time step. Overall, this results in a more stable IWP between different realizations (4a and c) due to radiative cooling of the cloud.

The profile of N_i for STD in Fig. 4a illustrates the principle of that immersion freezing representation prescribing N_i diagnostically: for STD, within the cloud and ca. 100 m below it, N_i has the prescribed minimum value of 200 m^{-3} . Down to the surface, the concentration is lower but constant, which is caused by steady sedimentation of ice crystals from above combined with fewer grid points reaching the threshold ice supersaturation. Q_i has the maximum values at the cloud bottom (Fig. 4b), which is commonly observed in Arctic mixed-phase clouds (Shupe et al., 2008). Since no cold-phase collection processes are active in these simulations, ice crystal mass the mass of single ice crystals can only grow by deposition. The total mass of ice however is affected also by transport processes like sedimentation. The vertical distribution of N_i and Q_i in F22-F23 is similar to STD (Fig. 4c and d). However, both Q_i and N_i increase by larger rates throughout the simulation time for F22-F23, which can also be seen in the IWP and ICNB values (Fig. 3b and c). Towards the end of the simulation time, F22-F23 ice values are about half of STD. Even though ice nucleation depends on temperature in F22 the temperature in F23, N_i is quite homogeneously distributed throughout the cloud (Fig. 4c). We explain this by the uniform stratification of the cloud and the subtraction of N_i from INPC (Eq. 2a) in the scheme, which homogenizes N_i vertically over time.

3.2 Sensitivity studies Comparison to observations

LWP as calculated in MIMICA is substantially higher than the 75th percentile of the observed values, irrespective of the treatment of ice nucleation (Fig. 3a). Stevens et al. (2018) found this already in their model inter-comparison study, where MIMICA was amongst the models with the highest LWP. The LWP exceeded the observations for simulations similar to ours with no prognostic aerosol treatment but a simplified treatment of aerosol activation (note however, that the MIMICA-simulations in Stevens et al., 2018 included snow and graupel). MIMICA-simulations, where aerosol is modeled prognostically, yielded results closer to the observational range in the study by Stevens et al. (2018). The IWP for STD lies within the interquartile range of the observations (Fig. 3b) which was found in Stevens et al., 2018 as well. The minimum N_i in STD was chosen in order to yield ice masses in the cloud similar to the observations. For the F23 simulations, IWP is lower than the 25th percentile of the observations. F23 however only represents immersion freezing, leading to a lower ice mass. We can expect that multiplication processes were present in the observed cloud, which would have led to a higher IWP compared to model simulations that do not represent SIP. In fact, Sotiropoulou et al. (2021) simulated the same case using MIMICA and including a description of ice multiplication from breakup during ice-ice collisions. Their results show an increase in IWP by a factor of 2 to 3 when breakup is activated in the model. Adjusting our simulated IWP accordingly would result in values corresponding to the observed IWP for F23. LWP is decreased by approximately $25\text{-}35 \text{ g m}^{-2}$ in simulations with ice multiplication in Sotiropoulou et al. (2021). This would bring our modeled LWP values closer to the observations, but LWP would still be higher than observed, due to simplified aerosol activation as explained above.

One aspect that complicates the comparison of our simulations with observations is that we excluded snow and graupel. If snow and graupel were included in the simulations, IWP might increase as riming converts liquid to frozen mass. On the other

hand, this might also lead to faster precipitation and thus depletion of liquid or frozen water.

Note that our goal was to test F23 rather than include all necessary processes in order to closely model the observations.

3.3 Comparison of F23 to interactive F62 implementation

310 F62 calculates the number of cloud droplets that freeze to ice crystals from the temperature-dependent INPC [m^{-3}] given in Fletcher (1962) (and shown by the black line in Fig. 1):

$$\text{INPC}(T) = 0.02 \cdot \exp(-\beta \cdot T) \quad (3)$$

with $\beta = 0.6/(1^\circ\text{C})$ and T in $^\circ\text{C}$. The changes in N_i , N_c , Q_i and Q_c are calculated according to Eq. 2. Note that this parameterization is only strictly valid for $-10 > T > -30^\circ\text{C}$, but we extrapolate it to the temperatures of the simulated cloud (dotted line in Fig. 1). Analogously to F23, freezing happens where $T < 0^\circ\text{C}$ and cloud droplets are present.

315 Figures 3b and D1 show that very little ice is produced when using the F62 ice nucleation scheme. We explain this by the subtraction of N_i from $\text{INPC}(T)$ since this only leads to considerable ice formation at the beginning of the simulation, when no ice is present yet, or in cases when the temperature decreases. This comparison between F23 and F62 illustrates the difficulty of simulating reasonable ice masses in warm mixed-phase clouds with conventional schemes that yield one INPC for one set
320 of environmental conditions. Drawing from a distribution of INPCs according to F23 leads to substantially larger ice masses, and these might even be multiplied if, e.g., secondary ice processes would also be considered (see discussion in Sect. 3.2).

3.4 Sensitivity studies of F23

To investigate the sensitivity of the simulated cloud to the characteristics of the F22-F23 scheme, the following parameters (summarized in Tab. 2) were varied: i. the median and standard deviation of the INPC distribution (Secs. 3.4.1 and 3.4.2); ii.
325 the size of the temperature bins (Sec. 3.4.3 Sect. 3.4.3); iii. the frequency of drawing (Sec. 3.4.4 Sect. 3.4.4); iv. the resolution of the model domain (Sec. 3.4.5) Sect. 3.4.5). The sensitivity tests i. mean that we cover a wider spectrum of INPC RFDs than the one defined in Sect. 2.1 and shown in Fig. 1.

3.4.1 Median of the distribution

The median ($\exp(\mu)$) of the INPC RFD is multiplied by a factor (0.5-1.5) shifting the entire distribution in Fig. 1 up or down,
330 without changing the standard deviation. Having more INPs (higher median) or fewer INPs (lower median) impacts the amount of ice formed in the cloud. The effect can be seen from the modeling results of IWP (Tab. 3; Fig. 5), when increasing/decreasing the median by 25% or 50%, IWP increases/decreases accordingly. The vertical profiles exhibit this symmetry even more clearly with linear N_i and Q_i increases/decreases (Fig. 6a and b) and all changes are significant. The significance of differences in IWP between simulations is tested with a two-sided Kolmogorov-Smirnov test at the 95% level. Changes in vertical profiles
335 are tested with a two-sided t-test at the 95% level. It is expected that all variables concerning ice crystals increase (decrease) with increased (decreased) median INPC, since more (fewer) INPs lead to more (fewer) cloud droplets freezing. The change is

Table 2. Overview of sensitivity studies

Simulation name	Abbreviation	Frequency of drawing from RFD	Horizontal grid spacing	Minimum vertical grid spacing	Multiplicator of RFD Median	RFD Standard deviation	Size of temperature-bins
standard ^a	STD	-	62.5 m	7.5 m	-	-	-
baseline	F22-F23 F22-F23	every Δt^b	62.5 m	7.5 m	1	1.37	1°C
median 1.5	M1.5	every Δt	62.5 m	7.5 m	1.5	1.37	1°C
median 1.25	M1.25	every Δt	62.5 m	7.5 m	1.25	1.37	1°C
median 0.75	M0.75	every Δt	62.5 m	7.5 m	0.75	1.37	1°C
median 0.5	M0.5	every Δt	62.5 m	7.5 m	0.5	1.37	1°C
sigma 1.5	S1.5	every Δt	62.5 m	7.5 m	1	1.5·1.37	1°C
sigma 1.25	S1.25	every Δt	62.5 m	7.5 m	1	1.25·1.37	1°C
sigma 0.75	S0.75	every Δt	62.5 m	7.5 m	1	0.75·1.37	1°C
sigma 0.5	S0.5	every Δt	62.5 m	7.5 m	1	0.5·1.37	1°C
sigma 0	S0	-	62.5 m	7.5 m	1	- ^c	1°C
half degree	0.5Deg	every Δt	62.5 m	7.5 m	1	1.37	0.5°C
once 5 sec	5S	once per 5 sec	62.5 m	7.5 m	1	1.37	1°C
once 10 sec	10S	once per 10 sec	62.5 m	7.5 m	1	1.37	1°C
once 20 sec	20S	once per 20 sec	62.5 m	7.5 m	1	1.37	1°C
once 5 min	5M	once per 5 min	62.5 m	7.5 m	1	1.37	1°C
once 60 min	60M	once per 60 min	62.5 m	7.5 m	1	1.37	1°C
delay ^d	D-10S-5M	-, once per 10 sec, once per 5 min	62.5 m	7.5 m	1	1.37	1°C
low resolution	F22-F23 LR	every Δt	125 m	15 m	1	1.37	1°C

^a Simulation with diagnostic N_i , no interactive ice nucleation parameterization.

^b Time step

^c In this case, no distribution is used, but the median of the distribution is used for all freezing cases.

^d Simulation where ice nucleation is started after two hours, first with a drawing frequency of every 10 seconds, then after an additional two hours the drawing frequency is decreased to 5 minutes.

linear, since because the median is logarithmized in the formula's exponent (see Eq. 1). No change in the vertical distribution of cloud droplet concentration is apparent (not shown).

3.4.2 Standard deviation of the distribution

340 The standard deviation (σ) of the RFD determines the variability of the INP concentration. The wider the distribution, the larger the variability of drawn INPCs. For the modeled cloud, a larger variability results in substantially and significantly increased IWP, N_i and Q_i while a lower variability results in significantly smaller values (Fig. 7 and Fig. 8). The changes are exponential with linear changes of σ , since σ is in the exponent in the INPC RFD (Eq. 1). These results emphasize that it is the high large INPCs that dominate ice formation in F22. Ice F23. Increased ice formation triggered by high large INPCs could lead to cloud glaciation and subsequent cloud dissipation in colder clouds, if ice crystals grow on at the expense of liquid droplets due to the WBF process. A high N_i can also be relevant for In other simulations including secondary ice processes, where N_i is enhanced by for example, mechanical splintering or break-up of ice crystals (e.g., Field et al., 2016). For example, a

345

Table 3. The three quartiles (25th percentile: P₂₅, etc.) of IWP for all sensitivity studies for the final four ~~simulationed~~-simulated hours (8-12 h) and differences relative to ~~F22-F23~~ (Δ ~~F22F23~~) or STD (Δ STD). Values in g m⁻². Simulations with significant differences to ~~F22-F23~~ (STD) are highlighted with an asterisk. Significance was assessed with a two-sided Kolmogorov-Smirnov test at the 95% level. D-10S-5M is not included, because values are similar to 5M or 60M.

Simulation	IWP	Δ F22F23 IWP	Δ F22F23 IWP	Δ F22F23 /
	P ₂₅	Δ STD	P ₅₀	Δ STD
	2.6	-	2.8	-
F22-F23				
M1.5 *	3.7	1.1	4.0	1.2
M1.25 *	3.4	0.8	3.5	0.7
M0.75 *	2.0	-0.6	2.2	-0.6
M0.5 *	1.4	-1.2	1.5	-1.3
S1.5 *	16.8	14.2	17.3	14.5
S1.25 *	7.3	4.7	7.8	5.0
S0.75 *	0.9	-1.7	1.0	-1.8
S0.5 *	0.4	-2.2	0.4	-2.4
S0 *	0.1	-2.5	0.1	-2.7
0.5Deg	2.6	-	3.0	0.2
5S *	2.1	-0.5	2.2	-0.6
10S *	1.8	-0.8	1.9	-0.9
20S *	1.5	-1.1	1.7	-1.1
5M *	1.2	-1.4	1.3	-1.5
60M *	1.2	-1.4	1.3	-1.5
	1.8	-0.8	1.9	-0.9
F22-F23 LR *				
STD	6.7	-	6.8	-
STD LR *	6.3	-0.4	6.5	-0.3

high N_i can be relevant to even further enhance N_i . For example, Yano et al. (2016) report a critical $N_{i,crit}$ which can lead to an explosive enhancement of the ~~number of ice crystals~~ice crystal number. This $N_{i,crit}$ might only be reached if there is a possibility to draw ~~high INPCs~~. If high large INPCs with F23. If large INPCs become less probable (smaller σ), IWP, $N_{i,c}$ and Q_i decrease. This is also apparent when analyzing the simulation without an INPC distribution, using the RFD's median value at all time steps (green line in Figs. 7, 8a and c). All ~~ice variables~~ice variables (IWP, $N_{i,c}$ and Q_i) have the lowest values for this run (see Table 3). ~~So using realistic mean~~Using realistic median INPCs at the rather high temperature of the simulated case leads to almost no ice formation ~~Only once~~(see also Sect. 3.3 where the INPCs are much larger than the median of the F23 RFD, but almost no ice is produced). Once an INPC distribution is added, considerable ice is formed. Excluding negative

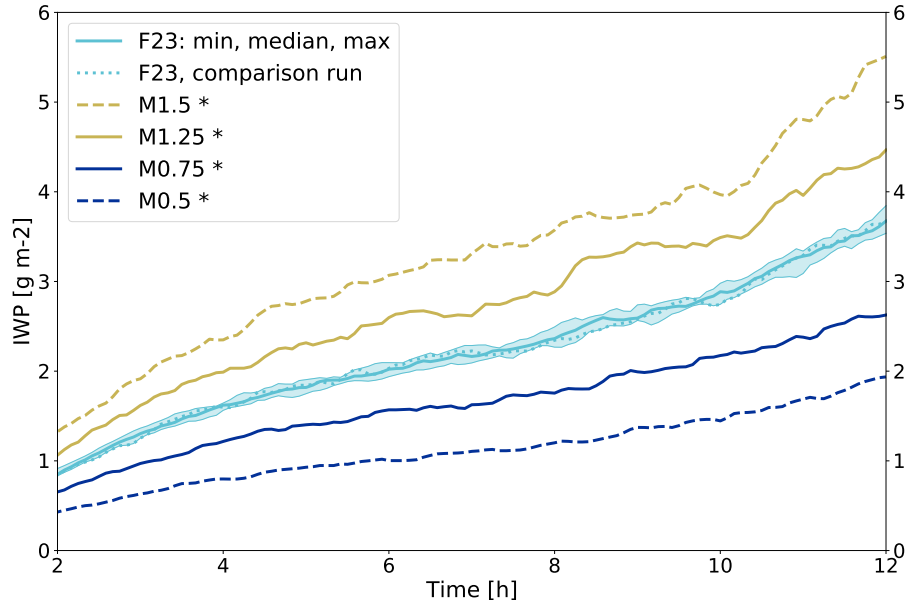


Figure 5. Domain-averaged IWP for 10 [F22-F23](#) simulations (cyan; median with min/max envelope, comparison run used in Fig. 6 is shown as a dotted line). Four sensitivity runs where the median of the RFD was changed (yellow: [higher-increased](#) median INPC, blue: [lower-decreased](#) median INPC). Significance was assessed with a two-sided Kolmogorov-Smirnov test at the 95% level. Significant differences to [F22-F23](#) are [marked-indicated](#) with an asterisk.

ΔN_i (Eq. 2a) causes N_i to progressively increase even without decreasing cloud temperature. Such increases can be expected from time-dependent immersion freezing.

It is remarkable that the large increase in ice for S1.5 even leads to changes in N_c and Q_c (Fig. 8b and d). The cloud bottom is elevated by ca. 100 m in comparison to the [F22-F23](#) case (Fig. 8b). This is probably because more cloud droplets freeze, leading to a depletion of unfrozen cloud droplets. Within the cloud, N_c is very similar for S1.5 and [F22-F23](#). However, Q_c for S1.5 is significantly smaller, indicating an enhanced WBF process resulting in liquid droplet evaporation.

3.4.3 Size of the temperature bins

For the [F22-F23](#) simulation, we draw from the INPC RFD defined on 1°C temperature bins [centered on whole degrees \(i.e., -0.5 to -1.5°C is the -1°C bin\)](#). Thus a change in temperature from e.g., -10.4 to -10.6°C shifts the INPC from the concentrations at -10°C to the concentrations at -11°C of the INPC distribution. Using smaller temperature bins [can be expected to make the parameterization](#), [we expect the parameterization to be](#) less sensitive to small temperature changes and lead to smaller changes in the drawn INPC concentrations. This effect was tested by decreasing the temperature [bins-bin range](#) from 1°C to 0.5°C (0.5Deg in Tab. 3). Figure 9 shows the IWP for a run with 0.5°C temperature binning. Overall, IWP for the 0.5Deg simulation does not significantly differ from the [F22-F23](#) runs. Until hour 8, IWP is slightly below the [F22-F23](#) case and between hours

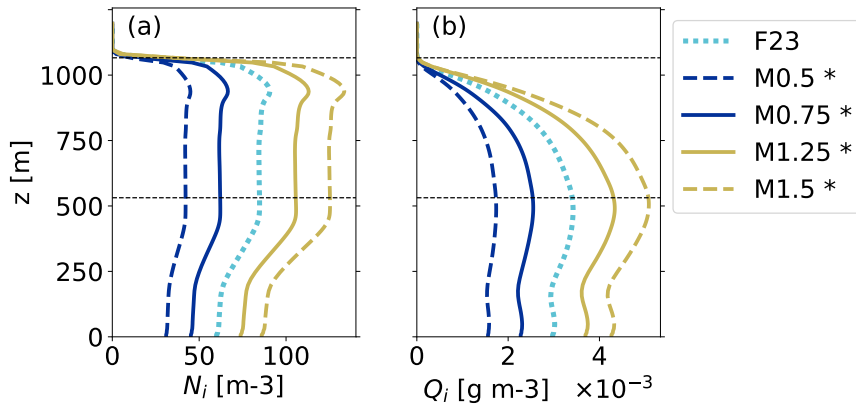


Figure 6. Profiles averaged over the domain and the simulation period of 8 - 12 hours: **(a)** N_i , **(b)** Q_i . The **F22-F23** comparison run is plotted in dotted cyan (see dotted line in Fig. 5), M0.5 and M0.75 in blue and M1.25 and M1.5 in yellow. Simulations with significant differences compared to **F22-F23** are **marked-indicated** with an asterisk (tested with a two-sided t-test at the 95% level). Horizontal dashed lines indicate the cloud's top and bottom in **F22-F23**.

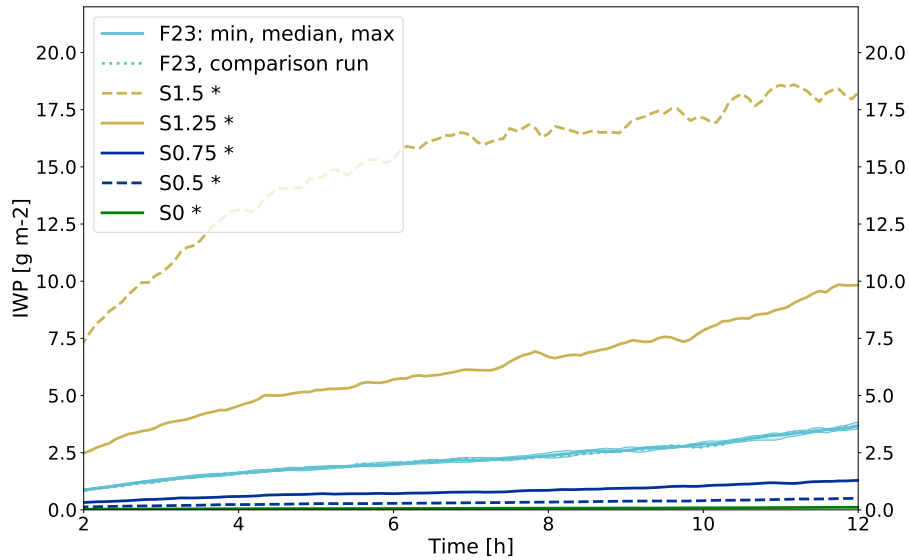


Figure 7. Domain-averaged IWP for 10 **F22-F23** simulations (cyan; median with min/max envelope, comparison run used in Fig. 8 is shown as a dotted line). Five sensitivity runs where the standard deviation of the RFD was changed (yellow: larger standard deviation, blue: smaller standard deviation, green: no standard deviation (**Only-only** median, **MS0**)). Significant differences to **F22-F23** are **marked-indicated** with an asterisk.

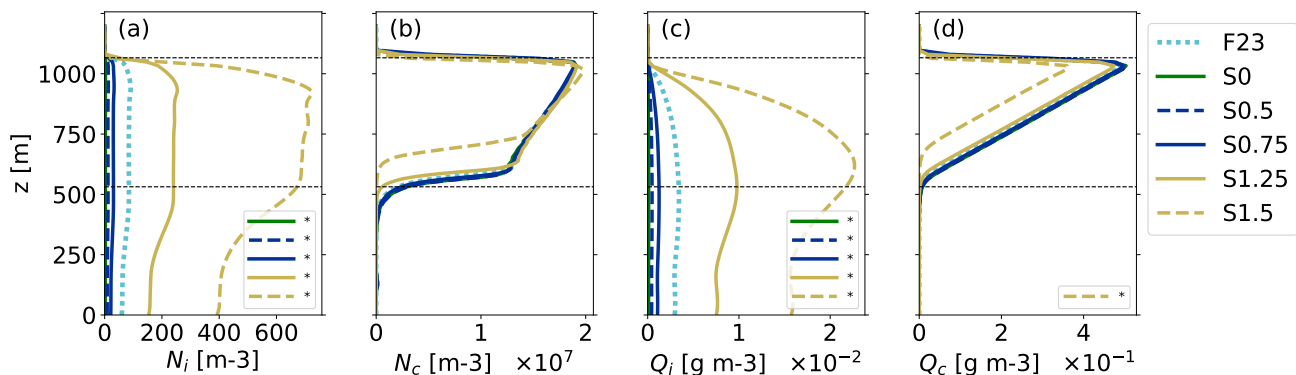


Figure 8. Profiles averaged over the domain and the simulation period of 8 - 12 hours: (a) N_i , (b) N_c , (c) Q_i and (d) Q_c . The F22-F23 comparison run is plotted in dotted cyan (see dotted line in Fig. 7), S0 in green, S0.5 and S0.75 in blue, S1.25 and S1.5 in yellow. Simulations that yielded significant differences compared to F22-F23 are shown in the respective variable's legend in the subplots (a)-(d). Horizontal dashed lines indicate the cloud's top and bottom in F22F23.

370 9 and 11, IWP is slightly larger. The averaged profiles for the final four simulated hours are shown in Fig. 10. None of the variables differ significantly between F22-F23 and 0.5Deg (see Tab. 3). Judging from these results, there is no compelling benefit in decreasing the size of the temperature bins (from 1°C to 0.5°C).

3.4.4 Frequency of drawing

The frequency of drawing a new value for the INPC ~~simulates the INPC variability over time, sets the length of the time period~~
 375 the drawn INPC is representative of the INPC at the grid point. The frequency of drawing is coupled to the model's temporal resolution, since the maximum frequency of drawing is restricted by the time step of the model. ~~Considering that one grid box within the cloud has the minimum dimensions of 62.5 m - 62.5 m - 7.5 m \approx 29,300 m³ and that the INP concentration can be assumed to be highly variable on even small time scales (Bigg, 1961) and smaller spatial scales, it is a plausible assumption to modulate INPC in each time step.~~ The sensitivity on to drawing frequency was tested by drawing the INPC once every five
 380 seconds (5S, see Tab. 3), once every ten seconds (10S), once every 20 seconds (20S), once every five minutes (5M) and once every 60 minutes (60M) instead of at every time step (F22F23: every 1-3 seconds). Freezing events still occur at every time step (according to Eq. 2), but within the respective time period (e. g., five seconds or 60 minutes), the INPC is constant at one grid point ~~for the time period. If the temperature at the grid point changes before the completion of the time period, a new INPC is drawn earlier.~~

385 IWP, N_i , and Q_i for the runs with lower drawing frequencies exhibit similar relative N_i increase increases over time as F22, F23 but have significantly lower absolute N_i concentrations (Figs values (Fig. 9 and 10). The ice variables profiles of ice variables also decrease as the frequency of drawing decreases (Fig. 10). This evolution can be explained by the subtraction of N_i at each time step. N_i at a grid point will not change between time steps for which $\text{INPC} < N_i$. Only when a newly drawn $\text{INPC} > N_i$,

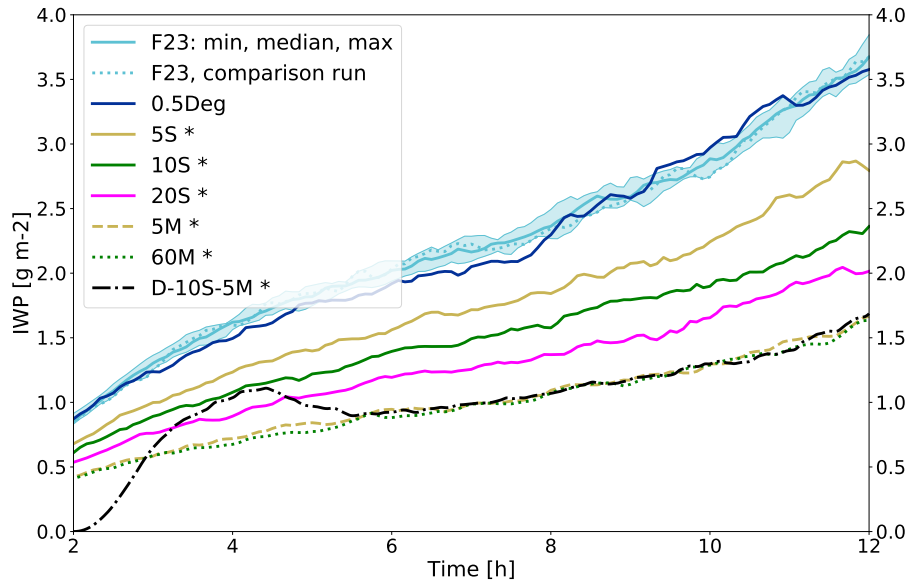


Figure 9. Domain-averaged IWP for 10 F22-F23 simulations (cyan: median with min/max envelope, comparison run used in Fig. 10 is shown as a dotted line). Six-Seven sensitivity tests (blue: 0.5Deg, yellow solid: 5S, green solid: 10S, magenta solid: 20S, yellow dashed: 5M, green dotted: 60M, black dash-dotted: D-10S-5M). Significant differences to F22-F23 are marked-indicated with an asterisk.

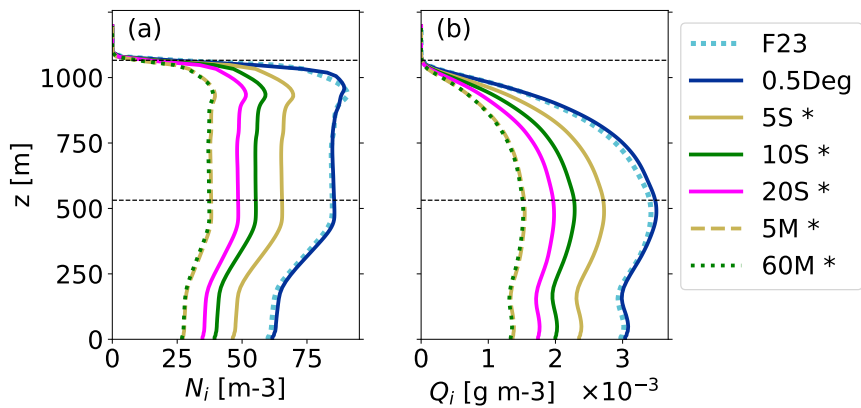


Figure 10. Profiles averaged over the domain and the simulation period of 8 - 12 hours: (a) N_i , (b) Q_i . One F22-F23 run in dotted cyan (see dotted line in Fig. 9), 0.5Deg in blue, 5S in yellow solid, 10S in green solid, 20S in magenta solid, 5M in yellow dashed, 60M in green dotted. Simulations with significant differences compared to F22-F23 are marked-indicated with an asterisk. Horizontal dashed lines indicate the cloud's top and bottom in F22-F23.

new ice is formed at the grid point. An exception is if there is a sink for N_i at the grid point (e.g., sedimentation, ~~aggregation,~~
390 ~~sublimation, or~~ advection) and N_i becomes smaller than INPC before the next draw of INPC, since then INPC - N_i cloud
droplets will freeze. As the overall ~~chances-chance~~ of drawing INPC $\gg N_i \gg N_i$ is higher with higher drawing frequency, the
frequency of drawing new INPCs changes the amount of new ice formation and ice content in the cloud. Note that since large
INPC and the chance to draw this large INPC determine the ice in the cloud, this introduces an indirect time-dependency of the
scheme. The resulting ice in the cloud depends indirectly on the time until a large INPC value is drawn at a specific grid point.
395 Increasing the drawing frequency leads to increases in the ice variables that do not appear to converge (Figs. 9 and 10, and
Tab. 3). As stated above, the maximum drawing frequency is the time step of the model, but the fact that the resulting cloud
ice diverges with increased drawing frequency poses a limitation of F23. Another feature apparent in Figs. 9 and 10, as well as
Tab. 3 is that the ice variables converge for drawing frequencies of five minutes or larger. ~~This is likely the average time it takes~~
~~for temperature to change at the grid points for the simulated stratiform cloud. The sensitivity to drawing frequency may be~~
400 ~~different for different cloud types. For example, in convective clouds the sensitivity could be very low because the temperature~~
~~changes more quickly than in the presented stratiform cloud, which leads to a high frequency of draws no matter which drawing~~
~~frequency is chosen in the scheme~~
The simulation D-10S-5M in Fig. 9 is a run where no ice nucleation is applied during the first two hours of the simulation. After
that, F23 is called with a drawing frequency of 10 seconds for two hours, and for the final eight hours, the drawing frequency
405 was set to five minutes. The simulation is not included in Fig. 10 and Tab. 3 since it results in the same values as 5M or 60M.
D-10S-5M shows that the current drawing frequency determines the amount of ice in the cloud.
It is important to investigate how the ice content reacts on very high and low drawing frequencies (asymptotic behavior).
In this study we are, however, constrained by the model setup. Yet, we can expect that processes other than heterogeneous
ice nucleation would limit ice production for high drawing frequencies in more realistic model setups. For example, ice
410 multiplication would lead to a quick increase in N_i , which would result in small or absent ice nucleation due to the subtraction
of N_i according to Eq. 2a. We assume that the converging behavior of the ice mass for low drawing frequencies (no difference
between 5M and 60M) is caused by other components of the model than the heterogeneous ice nucleation scheme. If there
were no other processes affecting ice number, decreasing the drawing frequency can be expected to lead to decreasing ice in
the cloud.

415 3.4.5 Resolution of the domain

The spatial resolution of the model domain affects the ~~F22-F23~~ scheme in a similar way as the frequency of drawing, by
changing the number of draws of INPC for the same cloud. However, a change in the model resolution impacts all parts of
the model, including microphysical processes. The sensitivity of the LES at a lower resolution is tested by doubling the grid
spacing in all three dimensions while the domain volume remains constant (STD LR and ~~F22-F23~~ LR). Note that this will also
420 lead to a doubling of the model time step, since it is calculated dynamically to satisfy the CFL criterion. Testing the scheme
on a more coarse grid is important, since the because one goal for the new parameterization is that it can be ~~used-in-adapted to~~
larger-scale models where the resolution will be much coarser than in large-eddy simulations. Lowering the resolution leads to

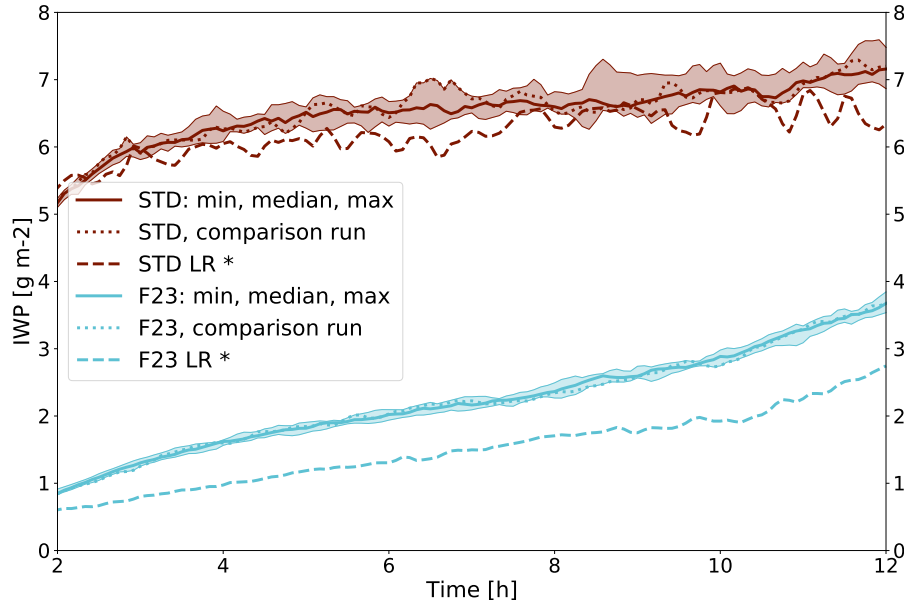


Figure 11. Domain-averaged IWP for 10 STD (red; median with min/max envelope, comparison run used in Fig. 12 is shown as a dotted line) and 10 F22-F23 simulations (cyan; median with min/max envelope, comparison run used in Fig. 12 is shown as a dotted line). One run with half of the entire resolution respectively (dashed lines). Significant differences to STD or F22-F23 are marked indicated with an asterisk.

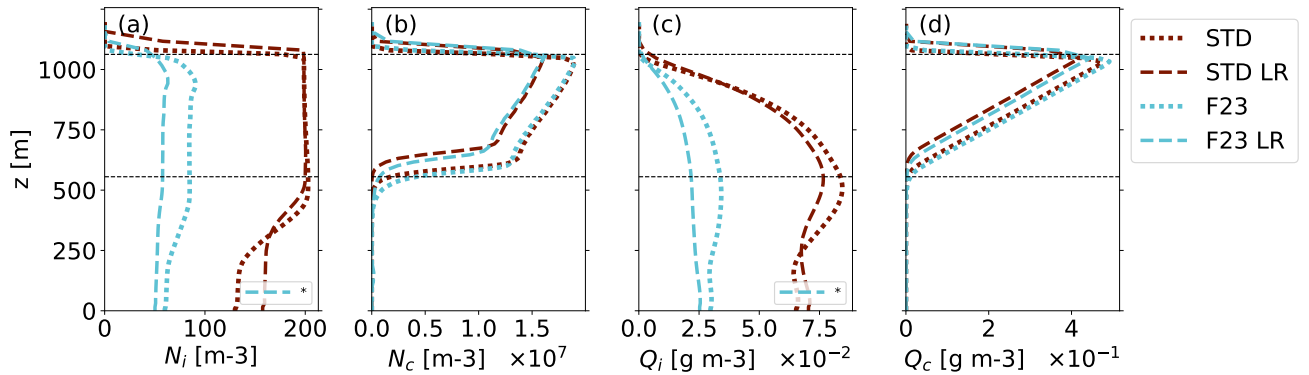


Figure 12. Profiles averaged over the domain and the simulation period of 8 - 12 hours: (a) N_i , (b) N_c , (c) Q_i and (d) Q_c . One STD in red dotted, one F22-F23 run in cyan dotted (see dotted lines in Fig. 11), STD LR in red dashed and F22-F23 LR in cyan dashed. Simulations that F23 LR in (a) and (c) yielded significant differences compared to F22 are shown in the respective variable's legend. Horizontal dashed lines indicate the cloud's top and bottom in STD.

significantly lower IWP for both the STD LR and F22-F23 LR simulation (Fig. 11). IWP is affected more in the simulation with the F22-F23 scheme. The vertical profiles of the cloud droplet variables (Figs. 12b and d) show non-significant, but consistent

425 decreases in N_c (Fig. 12b), as well as Q_c (Fig. 12d) for both runs with lower resolution. The decrease might be caused by changes in mixing processes, e.g., entrainment at the cloud borders, due to the change in grid size. N_i within the cloud is fixed to 200 m^{-3} for STD LR and STD (Fig. 12a) as per definition (see Sect. 2.2). Nevertheless, Q_i is lower for STD LR compared to STD (Fig. 12c). This can be explained by the decrease in Q_c and thus a less efficient WBF process providing a smaller mass flux from liquid droplets to ice crystals. For ~~F22~~ F23 LR, all variables shown in Fig. 12 decrease - for N_i and Q_i these changes are significant. The decrease in N_i can be explained by the smaller number of grid points in the domain as well as a coarser temporal resolution. INPCs will be drawn at only ~~one-eighth~~ one-eighth of the number of grid points ~~in F22 and only about half as often in F23~~ LR and thus large INPCs will be ~~picked~~ drawn less often than for ~~F22~~ F23. The results shown in Figs. 11 and 12 underline the ~~conclusion from Sec. 3.4.2 that the highest INPCs have~~ conclusions from Sect. 3.4.2 and Sect. 3.4.4 that the possibility to draw very large INPCs has the strongest effect on overall N_i .

435 4 Conclusions

A novel parameterization of immersion freezing that takes into account the observed variability of ice nucleating particles is presented. The observed INPC variability is reproduced by random drawing from an INPC relative frequency distribution that depends on temperature. ~~Since the F22 parameterization is based on long-term and wide-spread atmospheric INPC observations in a broad temperature range, it~~ This means that the INP population at a specific grid point is represented by a new value at the chosen frequency of drawing. If the newly drawn INPC exceeds the present N_i , additional ice is formed. The F23 parameterization is valid for the entire temperature range of heterogeneous immersion freezing between 0 and -38°C . ~~F22~~ F23 has the additional advantage that it does not require information on the present bulk aerosol from the atmospheric model, which makes it easy to implement and use in many different models. The main goal of this study was to test the general approach of representing immersion freezing by random drawing from an INPC distribution, as opposed to using traditional parameterizations that yield one INPC for the given temperature like, e.g., F62 (Fletcher, 1962).

We tested the parameterization for the large-eddy simulation of a mixed-phase Arctic stratocumulus cloud case with MIMICA. We used this case as a test bed for ~~F22~~ F23 because aerosol characteristics in the Arctic are largely unknown and this lack of information on aerosol bulk properties makes it challenging to use “classical” ~~aerosol-based~~ aerosol-aware freezing schemes. Moreover, it might be important to consider the whole range of possible INPCs in the Arctic summer where warm mixed-
450 phase clouds are frequently observed. ~~It was~~ The simulations with F23 lead to less cloud ice than was observed, but our model setup does not include graupel and snow as well as ice nucleation modes other than immersion freezing, or secondary ice processes. The latter has been shown to increase IWP by a factor of 2-3 leading to the observed values in MIMICA-simulations of the same case by Sotiropoulou et al. (2021). Through our sensitivity tests, we found that the simulated IWP, N_i , and Q_i of the cloud depend linearly on the median of the ~~relative frequency distribution~~ RFD that describes the INPC variability, and exponentially on the distribution’s standard deviation. The large ~~dependency~~ dependence on the standard deviation of the distribution is especially interesting, as it implies that the amount of ice in the modeled cloud is particularly sensitive to ~~high~~ large INP concentrations. The possibility of drawing high large INPC can influence cloud glaciation for colder cases caused by

the WBF process and secondary ice processes when $N_{i,crit}$ is reached (Yano et al., 2016). The relevance of randomly drawing INPC from a distribution is highlighted by the much lower IWP, $N_{i,c}$, and Q_i when applying the Fletcher parameterization F62 or simply using the median INP concentration (i.e., no INPC distribution). ~~In addition to the distribution's median and standard deviation~~ This emphasizes that it is the rare, but large INPCs that control the freezing in the cloud, rather than the median INPC values. Additionally, the frequency of drawing a new INPC has a significant impact on the ice variables \bar{r} since it is when a new, larger INPC is drawn that ~~most additional~~ ice is formed (Eq. 2a). The ~~lower-higher~~ the frequency of drawing, the ~~lower higher~~ the ice content in the cloud. However, drawing every five minutes or less often (e.g., every 60 minutes) ~~leads to results in~~ a similar amount of ice in the cloud. ~~This saturation effect depends on the modeled cloud type and the temperature fluctuations within the cloud. Lower resolution of the model domain affects both the ice and cloud droplet concentrations within the cloud, as well as mixing ratios. This sensitivity should be considered for possible implementations of the scheme into models with different resolutions. A qualitative comparison with similar simulations (ASCOS in MIMICA) by Sotiropoulou et al. (2021) or Stevens et al. (2018) shows slightly lower IWP for the baseline F22 setup. In contrast to the two studies, we have not included~~ graupel and snow in our simulations, thus we expect lower IWP. This means that our results are in a reasonable range with previous studies The high sensitivity of simulated cloud ice to an increased possibility to draw large INPC values (as tested by the increased standard deviation of the RFD, high drawing frequency, and higher spatial and temporal model resolution) poses the challenge of choosing the parameters (RFD standard deviation, and drawing frequency) for F23 while being in accordance with INPC observations. Further investigations are necessary to specify these parameters in order to apply the parameterization to other cases or in other models.

The scheme's independence from aerosol information in the atmospheric model is a strength \bar{r} but can be a limitation. ~~F22 represents the measurements (in this case maritime background measurements) behind the given INPC RFD that~~ The proposed INPC distribution of F23 may not be representative ~~for~~ of distinct scenarios, e.g., a Sahara dust outbreak. The RFD would need to be updated with one that is based on INPC observations specific ~~for the event or location~~ to an area or event of interest. However, the parameterization is flexible ~~to and can~~ be adapted to different ~~sets of observational INPC from other locations or years~~ INPC observations. To represent several sources or source regions at the same time in a model, different RFDs could be used depending on the location (remote vs. continental INP as an example). The independence to modeled aerosol might require updating the RFD when simulating future scenarios including changes in aerosol or INP concentrations. Some degree of autocorrelation between subsequent random draws from the INPC RFD in time and space could be added to the scheme in the future. ~~It~~ However, it is not clear what degree of autocorrelation would be physically reasonable. Since our study is based on one rather warm Arctic stratocumulus case, the parameterization should be tested and validated for other conditions and case studies in the future, especially for lower in-cloud temperatures. Additionally, ~~it~~ F23 should be tested ~~how F22 performs~~ in LES-models other than MIMICA ~~or larger scale and in larger scale~~ models. The intention of this study was to ~~learn illuminate~~ what including randomness in INPC ~~can lead leads~~ to. We ~~showed here show~~ that representing INP heterogeneity in an immersion freezing parameterization allows for a realistic simulation of an Arctic stratocumulus cloud, but are clearly left with remaining challenges.

In order to make it easier to use INPC observations in schemes like the one presented, measurements should be reported either

as individual ~~measurements~~ measurement points (e.g., as time series) ~~, or if aggregated~~ or, if aggregated, both with the average and standard deviation of the underlying log-normal distribution.

495 *Code and data availability.* The model output data presented in this study will be published at Zenodo after acceptance of the paper. Fortran code for the scheme is available from the authors upon request.

Author contributions. **Idea:** AW, LI **Prestudy:** ML, AW, LI **Conceptualisation:** LI, HF **Model implementation:** HF **Simulations:** HF **Analysis of the data and visualisation:** HF, LI **Writing:** HF **Review & editing:** All authors.

Competing interests. The authors declare that no competing interests are present.

500 *Acknowledgements.* H.C.F. and L.I. were supported by Chalmers Gender Initiative for Excellence (Genie). E.S.T. was supported by the Swedish Research Councils, FORMAS (2017-00564) and VR (2020-03497), and the Swedish Strategic Research Initiative Modelling the Regional and Global Earth system, MERGE. The computations were enabled by resources provided by the Swedish National Infrastructure for Computing (SNIC) at National Supercomputer Centre (NSC) partially funded by the Swedish Research Council through grant agreement no. 2018-05973. Hamish Struthers at LiU is acknowledged for assistance concerning technical and implementational aspects in making the code run on the Tetralith resources. We thank Annica M. L. Ekman for ~~valuable discussions~~ the valuable discussions and two anonymous reviewers for their constructive comments. We used the colormaps provided by Crameri et al. (2020). The research presented in this paper is a contribution to the strategic research area MERGE.

505

References

- Bertrand, J., Baudet, J., and Dessens, J.: Seasonal Variations and Frequency Distributions of Ice Nuclei Concentrations at Abidjan, West
510 Africa, *J. Appl. Meteorol. Climatol.*, 12, 1191–1195, [https://doi.org/10.1175/1520-0450\(1973\)012<1191:SVAFO>2.0.CO;2](https://doi.org/10.1175/1520-0450(1973)012<1191:SVAFO>2.0.CO;2), 1973.
- Bigg, E. K.: Natural Atmospheric Ice Nuclei, *Sci. Prog.*, 49, 458–475, <http://www.jstor.org/stable/43425202>, 1961.
- Bulatovic, I., Igel, A. L., Leck, C., Heintzenberg, J., Riipinen, I., and Ekman, A. M.: The Importance of Aitken Mode Aerosol Particles for
Cloud Sustainance in the Summertime High Arctic-A Simulation Study Supported by Observational Data, *Atmospheric Chem. Phys.*, 21,
3871–3897, <https://doi.org/10.5194/acp-21-3871-2021>, 2021.
- 515 Burrows, S. M., McCluskey, C. S., Cornwell, G., Steinke, I., Zhang, K., Zhao, B., Zawadowicz, M., Raman, A., Kulkarni, G., China, S.,
Zelenyuk, A., and DeMott, P. J.: Ice-Nucleating Particles That Impact Clouds and Climate: Observational and Modeling Research Needs,
Rev. Geophys., 60, e2021RG000 745, <https://doi.org/10.1029/2021RG000745>, 2022.
- Christiansen, S., Ickes, L., Bulatovic, I., Leck, C., Murray, B. J., Bertram, A. K., Wagner, R., Gorokhova, E., Salter, M. E., Ekman, A. M., and
Bilde, M.: Influence of Arctic Microlayers and Algal Cultures on Sea Spray Hygroscopicity and the Possible Implications for Mixed-Phase
520 Clouds, *J. Geophys. Res. Atmospheres*, 125, <https://doi.org/10.1029/2020JD032808>, 2020.
- Conen, F., Yakutin, M. V., Yttri, K. E., and Hüglin, C.: Ice Nucleating Particle Concentrations Increase When Leaves Fall in Autumn,
Atmosphere, 8, 202, <https://doi.org/10.3390/atmos8100202>, 2017.
- Cramer, F., Shephard, G. E., and Heron, P. J.: The misuse of colour in science communication, *Nat. Commun.*, 11, 5444,
<https://doi.org/10.1038/s41467-020-19160-7>, 2020.
- 525 de Boer, G., Morrison, H., Shupe, M. D., and Hildner, R.: Evidence of Liquid Dependent Ice Nucleation in High-Latitude Stratiform Clouds
from Surface Remote Sensors, *Geophys. Res. Lett.*, 38, <https://doi.org/10.1029/2010GL046016>, 2011.
- Field, P. R., Lawson, R. P., Brown, P. R. A., Lloyd, G., Westbrook, C., Moisseev, D., Miltenberger, A., Nenes, A., Blyth, A., Choulaton, T.,
Connolly, P., Buehl, J., Crosier, J., Cui, Z., Dearden, C., DeMott, P., Flossmann, A., Heymsfield, A., Huang, Y., Kalesse, H., Kanji, Z. A.,
Korolev, A., Kirchgaessner, A., Lasher-Trapp, S., Leisner, T., McFarquhar, G., Phillips, V., Stith, J., and Sullivan, S.: Chapter 7. Secondary
530 Ice Production - Current State of the Science and Recommendations for the Future, *Meteorol. Monogr.*, pp. AMSMONOGRAPHS-D–
16–0014.1, <https://doi.org/10.1175/AMSMONOGRAPHS-D-16-0014.1>, 2016.
- Fletcher, N.: *The physics of rainclouds*, Cambridge University Press, 1962.
- Flyger, H. and Heidam, N. Z.: Ground Level Measurements of the Summer Tropospheric Aerosol in Northern Greenland, *Journal of Aerosol
Science*, 9, 157–168, [https://doi.org/10.1016/0021-8502\(78\)90075-7](https://doi.org/10.1016/0021-8502(78)90075-7), 1978.
- 535 Fu, Q. and Liou, K. N.: Parameterization of the Radiative Properties of Cirrus Clouds, *J. Atmospheric Sci.*, 50, 2008–2025, 1993.
- Hartmann, M., Blunier, T., Brügger, S., Schmale, J., Schwikowski, M., Vogel, A., Wex, H., and Stratmann, F.: Variation of Ice Nucleating
Particles in the European Arctic Over the Last Centuries, *Geophys. Res. Lett.*, 46, 4007–4016, <https://doi.org/10.1029/2019GL082311>,
2019.
- Ickes, L., Welti, A., and Lohmann, U.: Classical Nucleation Theory of Immersion Freezing: Sensitivity of Contact Angle Schemes to Ther-
540 modynamic and Kinetic Parameters, *Atmospheric Chem. Phys.*, 17, 1713–1739, <https://doi.org/10.5194/acp-17-1713-2017>, 2017.
- Isaac, G. A. and Douglas, R. H.: Frequency Distributions of Ice Nucleus Concentrations, *J. Rech. Atmos.*, 5, 1–4, 1971.
- Khvorostyanov, V. I. and Curry, J. A.: A New Theory of Heterogeneous Ice Nucleation for Application in Cloud and Climate Models,
Geophys. Res. Lett., 27, 4081–4084, <https://doi.org/10.1029/1999GL011211>, 2000.

- Khvorostyanov, V. I. and Curry, J. A.: Aerosol Size Spectra and CCN Activity Spectra: Reconciling the Lognormal, Algebraic, and Power
545 Laws, *J. Geophys. Res.*, 111, D12 202, <https://doi.org/10.1029/2005JD006532>, 2006.
- Li, G., Wieder, J., Pasquier, J. T., Henneberger, J., and Kanji, Z. A.: Predicting Atmospheric Background Number Concentration of Ice-
Nucleating Particles in the Arctic, *Atmospheric Chem. Phys.*, 22, 14 441–14 454, <https://doi.org/10.5194/acp-22-14441-2022>, 2022.
- Loewe, K., Ekman, A. M. L., Paukert, M., Sedlar, J., Tjernström, M., and Hoose, C.: Modelling Micro- and Macrophysical Contributors to
the Dissipation of an Arctic Mixed-Phase Cloud during the Arctic Summer Cloud Ocean Study (ASCOS), *Atmospheric Chem. Phys.*, 17,
550 6693–6704, <https://doi.org/10.5194/acp-17-6693-2017>, 2017.
- Marcolli, C., Gedamke, S., Peter, T., and Zobrist, B.: Efficiency of Immersion Mode Ice Nucleation on Surrogates of Mineral Dust, *Atmos.
Chem. Phys.*, 7, 5081–5091, <https://doi.org/10.5194/acp-7-5081-2007>, 2007.
- Matus, A. V. and L'Ecuyer, T. S.: The role of cloud phase in Earth's radiation budget, *J. Geophys. Res. Atmos.*, 122, 2559–2578,
<https://doi.org/10.1002/2016JD025951>, 2017.
- 555 Morrison, H. and Grabowski, W. W.: Modeling Supersaturation and Subgrid-Scale Mixing with Two-Moment Bulk Warm Microphysics, *J.
Atmospheric Sci.*, 65, 792–812, <https://doi.org/10.1175/2007JAS2374.1>, 2008.
- Niemand, M., Möhler, O., Vogel, B., Vogel, H., Hoose, C., Connolly, P., Klein, H., Bingemer, H., Demott, P., Skrotzki, J., and Leisner, T.:
A Particle-Surface-Area-Based Parameterization of Immersion Freezing on Desert Dust Particles, *J. Atmospheric Sci.*, 69, 3077–3092,
<https://doi.org/10.1175/JAS-D-11-0249.1>, 2012.
- 560 Ott, W. R.: A Physical Explanation of the Lognormality of Pollutant Concentrations, *J. Air Waste Manag. Assoc.*, 40, 1378–1383,
<https://doi.org/10.1080/10473289.1990.10466789>, 1990.
- Petters, M. D. and Wright, T. P.: Revisiting Ice Nucleation from Precipitation Samples, *Geophys. Res. Lett.*, 42, 8758–8766,
<https://doi.org/10.1002/2015GL065733>, 2015.
- Phillips, V. T. J., DeMott, P. J., and Andronache, C.: An Empirical Parameterization of Heterogeneous Ice Nucleation for Multiple Chemical
565 Species of Aerosol, *J. Atmos. Sci.*, 65, 2757–2783, <https://doi.org/10.1175/2007JAS2546.1>, 2008.
- Radke, L. F., Hobbs, P. V., and Pinnons, J. E.: Observations of Cloud Condensation Nuclei, Sodium-Containing Particles, Ice Nuclei
and the Light-Scattering Coefficient Near Barrow, Alaska, *J. Appl. Meteorol. Climatol.*, 15, 982–995, [https://doi.org/10.1175/1520-0450\(1976\)015<0982:OOCNS>2.0.CO;2](https://doi.org/10.1175/1520-0450(1976)015<0982:OOCNS>2.0.CO;2), 1976.
- Savre, J. and Ekman, A. M.: A Theory-Based Parameterization for Heterogeneous Ice Nucleation and Implications for the Simulation of Ice
570 Processes in Atmospheric Models, *J. Geophys. Res.*, 120, 4937–4961, <https://doi.org/10.1002/2014JD023000>, 2015a.
- Savre, J. and Ekman, A. M. L.: Large-Eddy Simulation of Three Mixed-Phase Cloud Events during ISDAC: Conditions for Persistent
Heterogeneous Ice Formation, *J. Geophys. Res. Atmospheres*, 120, 7699–7725, <https://doi.org/10.1002/2014JD023006>, 2015b.
- Savre, J., Ekman, A. M. L., and Svensson, G.: Technical Note: Introduction to MIMICA, a Large-Eddy Simulation Solver for Cloudy
Planetary Boundary Layers, *J. Adv. Model. Earth Syst.*, 6, 630–649, <https://doi.org/10.1002/2013MS000292>, 2014.
- 575 Schrod, J., Thomson, E. S., Weber, D., Kossmann, J., Pöhlker, C., Saturno, J., Ditas, F., Artaxo, P., Clouard, V., Saurel, J.-M., Ebert, M.,
Curtius, J., and Bingemer, H. G.: Long-Term Deposition and Condensation Ice-Nucleating Particle Measurements from Four Stations
across the Globe, *Atmos. Chem. Phys.*, 20, 15 983–16 006, <https://doi.org/10.5194/acp-20-15983-2020>, 2020.
- Seifert, A. and Beheng, K. D.: A Double-Moment Parameterization for Simulating Autoconversion, Accretion and Selfcollection, *Atmo-
spheric Res.*, [https://doi.org/10.1016/S0169-8095\(01\)00126-0](https://doi.org/10.1016/S0169-8095(01)00126-0), 2001.
- 580 Seifert, A. and Beheng, K. D.: A Two-Moment Cloud Microphysics Parameterization for Mixed-Phase Clouds. Part 1: Model Description,
Meteorol. Atmospheric Phys., 92, 45–66, <https://doi.org/10.1007/s00703-005-0112-4>, 2006.

- Shupe, M. D., Kollias, P., Persson, P. O. G., and McFarquhar, G. M.: Vertical Motions in Arctic Mixed-Phase Stratiform Clouds in: *Journal of the Atmospheric Sciences* Volume 65 Issue 4 (2008), *J. Atmos. Sci.*, 65, 1304–1322, <https://doi.org/10.1175/2007JAS2479.1>, 2008.
- Shupe, M. D., Persson, P. O., Brooks, I. M., Tjernström, M., Sedlar, J., Mauritsen, T., Sjogren, S., and Leck, C.: Cloud and Boundary Layer
585 Interactions over the Arctic Sea Ice in Late Summer, *Atmospheric Chem. Phys.*, <https://doi.org/10.5194/acp-13-9379-2013>, 2013.
- Solomon, A., Feingold, G., and Shupe, M. D.: The Role of Ice Nuclei Recycling in the Maintenance of Cloud Ice in Arctic Mixed-Phase Stratocumulus, *Atmospheric Chem. Phys.*, 15, 10 631–10 643, <https://doi.org/10.5194/acp-15-10631-2015>, 2015.
- Sotiropoulou, G., Sullivan, S., Savre, J., Lloyd, G., Lachlan-Cope, T., Ekman, A. M. L., and Nenes, A.: The Impact of Secondary Ice Production on Arctic Stratocumulus, *Atmospheric Chem. Phys.*, 20, 1301–1316, <https://doi.org/10.5194/acp-20-1301-2020>, 2020.
- 590 Sotiropoulou, G., Ickes, L., Nenes, A., and Ekman, A. M. L.: Ice Multiplication from Ice–Ice Collisions in the High Arctic: Sensitivity to Ice Habit, Rimed Fraction, Ice Type and Uncertainties in the Numerical Description of the Process, *Atmospheric Chem. Phys.*, 21, 9741–9760, <https://doi.org/10.5194/acp-21-9741-2021>, 2021.
- Stevens, R. G., Loewe, K., Dearden, C., Dimitrellos, A., Possner, A., Eirund, G. K., Raatikainen, T., Hill, A. A., Shipway, B. J., Wilkinson, J., Romakkaniemi, S., Tonttila, J., Laaksonen, A., Korhonen, H., Connolly, P., Lohmann, U., Hoose, C., Ekman, A. M. L., Carslaw, K. S., and
595 Field, P. R.: A Model Intercomparison of CCN-limited Tenuous Clouds in the High Arctic, *Atmospheric Chem. Phys.*, 18, 11 041–11 071, <https://doi.org/10.5194/acp-18-11041-2018>, 2018.
- Tjernström, M., Birch, C. E., Brooks, I. M., Shupe, M. D., Persson, P. O. G., Sedlar, J., Mauritsen, T., Leck, C., Paatero, J., Szczodrak, M., and Wheeler, C. R.: Meteorological Conditions in the Central Arctic Summer during the Arctic Summer Cloud Ocean Study (ASCOS), *Atmospheric Chem. Phys.*, 12, 6863–6889, <https://doi.org/10.5194/acp-12-6863-2012>, 2012.
- 600 Tjernström, M., Leck, C., Birch, C. E., Bottenheim, J. W., Brooks, B. J., Brooks, I. M., Bäcklin, L., Chang, R. Y.-W., de Leeuw, G., Di Liberto, L., de la Rosa, S., Granath, E., Graus, M., Hansel, A., Heintzenberg, J., Held, A., Hind, A., Johnston, P., Knulst, J., Martin, M., Matrai, P. A., Mauritsen, T., Müller, M., Norris, S. J., Orellana, M. V., Orsini, D. A., Paatero, J., Persson, P. O. G., Gao, Q., Rauschenberg, C., Ristovski, Z., Sedlar, J., Shupe, M. D., Sierau, B., Sirevaag, A., Sjogren, S., Stetzer, O., Swietlicki, E., Szczodrak, M., Vaattovaara, P., Wahlberg, N., Westberg, M., and Wheeler, C. R.: The Arctic Summer Cloud Ocean Study (ASCOS): Overview and Experimental Design,
605 *Atmospheric Chem. Phys.*, 14, 2823–2869, <https://doi.org/10.5194/acp-14-2823-2014>, 2014.
- Vali, G., DeMott, P. J., Möhler, O., and Whale, T. F.: Technical Note: A Proposal for Ice Nucleation Terminology, *Atmospheric Chem. Phys.*, 15, 10 263–10 270, <https://doi.org/10.5194/acp-15-10263-2015>, 2015.
- Wang, C. and Chang, J. S.: A Three-Dimensional Numerical Model of Cloud Dynamics, Microphysics, and Chemistry: 1. Concepts and Formulation, *J. Geophys. Res.*, 98, 14 827, <https://doi.org/10.1029/92JD01393>, 1993.
- 610 Wang, Y., Liu, X., Hoose, C., and Wang, B.: Different Contact Angle Distributions for Heterogeneous Ice Nucleation in the Community Atmospheric Model Version 5, *Atmospheric Chem. Phys.*, 14, 10 411–10 430, <https://doi.org/10.5194/acp-14-10411-2014>, 2014.
- Welti, A., Müller, K., Fleming, Z. L., and Stratmann, F.: Concentration and Variability of Ice Nuclei in the Subtropical Maritime Boundary Layer, *Atmospheric Chem. Phys.*, 18, <https://doi.org/10.5194/acp-18-5307-2018>, 2018.
- Welti, A., Bigg, E. K., DeMott, P., Gong, X., Hartmann, M., Harvey, M., Henning, S., Herenz, P., Hill, T., Hornblow, B., Leck, C., Löffler, M., McCluskey, C., Rauker, A. M., Schmale, J., Tatzelt, C., van Pinxteren, M., and Stratmann, F.: Ship-Based Measurements of Ice Nuclei Concentrations over the Arctic, Atlantic, Pacific and Southern Ocean, *Atmospheric Chem. Phys.*, pp. 1–22, <https://doi.org/10.5194/acp-2020-466>, 2020.
- Wex, H., Huang, L., Zhang, W., Hung, H., Traversi, R., Becagli, S., Sheesley, R. J., Moffett, C. E., Barrett, T. E., Bossi, R., Skov, H., Hünerbein, A., Lubitz, J., Löffler, M., Linke, O., Hartmann, M., Herenz, P., and Stratmann, F.: Annual Variability of Ice-Nucleating

620 Particle Concentrations at Different Arctic Locations, Atmospheric Chem. Phys., 19, 5293–5311, <https://doi.org/10.5194/acp-19-5293-2019>, 2019.

Yano, J.-I., Phillips, V. T. J., and Kanawade, V.: Explosive Ice Multiplication by Mechanical Break-up in Ice–Ice Collisions: A Dynamical System-Based Study, Q. J. R. Meteorol. Soc., 142, 867–879, <https://doi.org/10.1002/qj.2687>, 2016.

Appendix A: MIMICA LES model description

625 The MIMICA LES solves a system of non-hydrostatic anelastic equations and represents cloud microphysics through a two-moment bulk microphysics scheme. The prognostic variables are number concentrations and mass mixing ratios of up to five represented hydrometeors: cloud droplets, ~~rain drops~~raindrops, cloud ice, snow, and graupel. All hydrometeor mass distributions are regular ~~gamma-distributions~~gamma distributions and the hydrometeors' terminal fall speeds are calculated from simple power laws dependent on their diameters. Warm microphysical processes are modeled according to Seifert and Beheng (2001) and Seifert and Beheng (2006), while collection processes involving frozen hydrometeors and resulting in the hydrometeors sticking together follow Wang and Chang (1993). MIMICA represents the following cold collection processes: i. riming of ice crystals and graupel by cloud droplets (resulting in graupel); ii. riming of ice crystals, graupel ~~and snow flakes by rain drops~~, and snowflakes by raindrops (resulting in graupel); iii. autoconversion of ice crystals to snow; iv. self-collection of ~~snow flakes~~snowflakes; v. collection of cloud droplets by snow (resulting in snow); vi. growth of a ~~snow flake~~snowflake by aggregating ice crystals; vii. collection of snow by graupel (resulting in graupel). Cloud condensation nuclei (CCN) activation is described following Khvorostyanov and Curry (2006), which is based on a simple power-law depending on modeled supersaturation and a prescribed background CCN concentration. It is possible to describe aerosol prognostically in MIMICA including activation as CCN. The supersaturation is solved pseudo-analytically following Morrison and Grabowski (2008). In the standard version of MIMICA, primary ice formation is represented by maintaining a constant ice crystal number concentration (N_i) within the cloud. However, it is also possible to choose an interactive ice nucleation scheme. ~~Secondary ice formation is not taken into account in this study since the focus is on primary ice formation.~~ Radiation is calculated according to Fu and Liou (1993). The initial ice/liquid potential temperature profiles are randomly perturbed in order for convection to develop ~~quicker~~more quickly. Consequently, any two simulations will yield different results, even if all parameters are held constant.

Appendix B: Averaged Q-tendency profiles for STD vs. ~~F22~~F23

645 Figure B1 shows tendencies relevant to the Wegener–Bergeron–Findeisen process (WBF), averaged over the domain and entire simulation time for STD and F23: condensation (positive values) and evaporation (negative values) for liquid water, $Q_l = Q_c + Q_r$, in Fig. B1a and deposition (positive values) and sublimation (negative values) for ice crystals, Q_i , in Fig. B1b. More deposition and evaporation occur in STD, illustrating the WBF process with a mass transfer from liquid to frozen water.

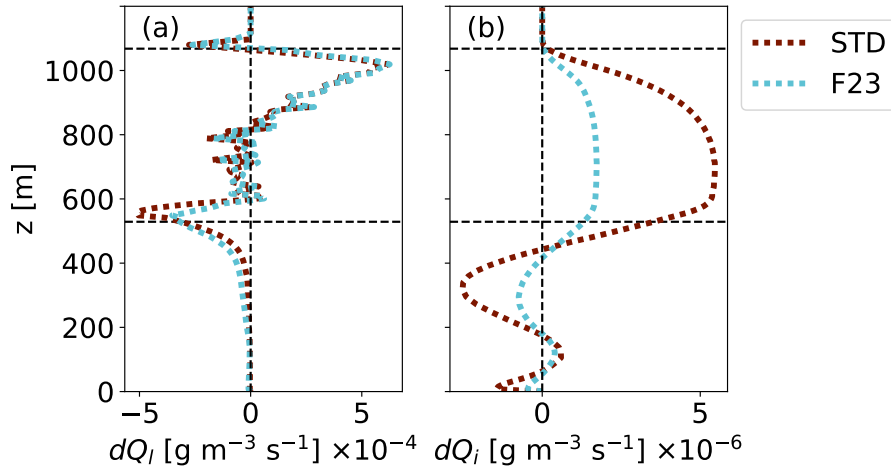


Figure B1. Profiles of WBF tendencies averaged over the domain and the entire simulation period: (a) evaporation/condensation, $dQ_l = dQ_c + dQ_r$, (b) sublimation/deposition, dQ_i . One STD in red dotted, and one F23 run in cyan dotted (see dotted lines in Fig. 3). Horizontal dashed lines indicate the cloud's top and bottom in F23 during the last four hours of the simulation.

Appendix C: Averaged N-profiles for STD vs. F23

650 Figure C1 shows time- and domain-averaged profiles of the number concentrations and mixing ratios of ice and cloud droplets of ice, cloud droplets, and raindrops for STD and F23.

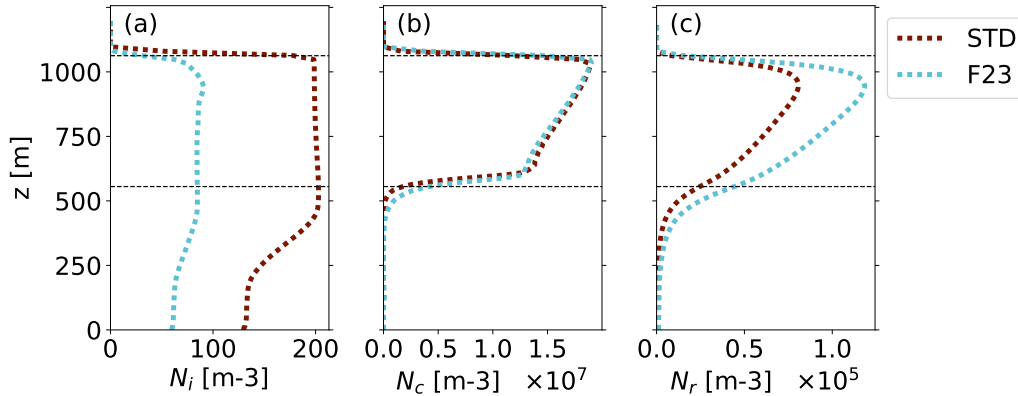


Figure C1. Profiles averaged over the domain and the simulation period of 8 - 12 hours: (a) N_i , (b) N_c , (c) N_r . One STD in red dotted, and one F22-F23 run in cyan dotted (see dotted lines in Fig. 3). Horizontal dashed lines indicate the cloud's top and bottom in STD.

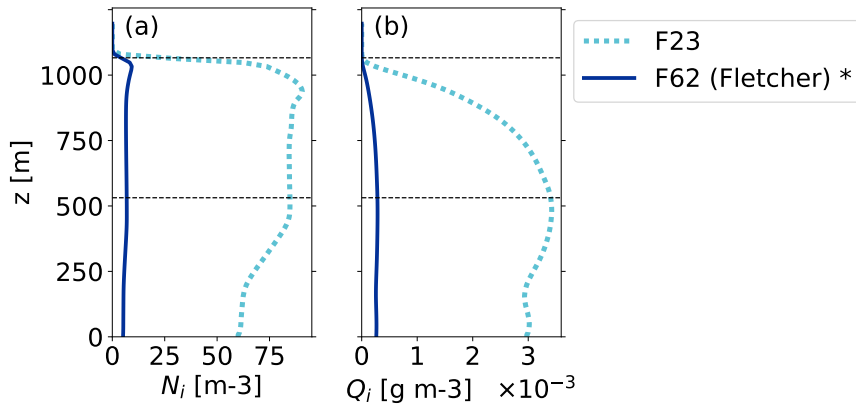


Figure D1. Profiles averaged over the domain and the simulation period of 8 - 12 hours: (a) N_i , (b) Q_i . The F23 comparison run is plotted in dotted cyan (see dotted line in Fig. 3), and one run with F62 in blue. Simulations with significant differences to F23 are indicated with an asterisk (tested with a two-sided t-test at the 95% level). Horizontal dashed lines indicate the cloud's top and bottom in F23.

Appendix D: Averaged N_i and Q_i profiles for F23 vs. F62

Figure D1 shows time- and domain-averaged profiles of the number concentration and mixing ratio of ice for F62 compared to F23.